# Electric field determination in transient plasmas: *in situ* & non-invasive methods

OPEN ACCESS
IOP Publishing
Plasma Sources Science and Technology
Plasma Sources Sci. Technol. **31** (2022) 073001 (21pp)
https://doi.org/10.1088/1361-6595/ac6e03

## Topical Review

# Electric field determination in transient plasmas: *in situ* & non-invasive methods

**Benjamin M Goldberg**[1,*], **Tomáš Hoder**[2] and **Ronny Brandenburg**[3,4]

[1] Lawrence Livermore National Laboratory, Livermore, CA 94550, United States of America
[2] Department of Physical Electronics, Faculty of Science, Masaryk University, Brno, Czech Republic
[3] Leibniz Institute for Plasma Science and Technology (INP), Greifswald, Germany
[4] Institute of Physics, University of Rostock, Rostock, Germany

E-mail: goldberg10@llnl.gov, hoder@physics.muni.cz and brandenburg@inp-greifswald.de

Received 20 December 2021, revised 28 March 2022
Accepted for publication 9 May 2022
Published 13 September 2022

**Abstract**

One of the primary basic plasma parameters within transient nonequilibrium plasmas is the reduced electric field strength, roughly understood as the ratio of the electrical energy given to the charged species between two collisions. While physical probes have historically been used for electric field measurements, recent advances in high intensity lasers and sensitive detection methods have allowed for non-invasive optical electric field determination in nearly any discharge configuration with time-resolution up to the sub-nanosecond range and sub-millimeter spatial resolution. This topical review serves to highlight several non-invasive methods for *in situ* electric field strength determination in transient plasmas ranging from high vacuum environments to atmospheric pressure and above. We will discuss the advantages and proper implementation of (i) laser induced fluorescence dip spectroscopy for measurements in low pressure RF discharges, (ii) optical emission spectroscopy based methods for nitrogen, helium or hydrogen containing discharges, (iii) electric field induced coherent Raman scattering, and (iv) electric field induced second harmonic generation. The physical mechanism for each method will be described as well as basic implementation and highlighting recent results.

Keywords: nonthermal plasma, gas discharge, electric field strength, optical emission spectroscopy, Stark polarization, coherent Raman scattering, EFISH

(Some figures may appear in colour only in the online journal)

## 1. Introduction

The world that we live in today would not be possible without physical plasmas and its applications. Plasma technology is a cross-sectional and key technology for the processing of materials and the manufacturing of a plethora of products. Its role remains often hidden, although it is an enabling and resource saving technology. Plasma processing is mandatory in the aerospace, automotive, steel, biomedical, textile, optics, plastics and paper industries. The ability of nonthermal plasmas to interact with sensitive materials and goods has extended the research and application to the treatment of liquids, organic tissues and wounds, which led to the field of plasma medicine. Other promising fields are nanomaterial synthesis, plasma metamaterials and photonic crystals, plasma chemical processing, plasma assisted combustion, plasma agriculture and cancer treatment. Nonthermal plasmas are also used, or are

* Author to whom any correspondence should be addressed.



 

under research in environmental protection technologies, in analytical chemistry as well as propulsion and flow control [1, 2]. Plasma operated at atmospheric pressure gained increasing attention within the last two decades. Its operation at open atmospheres enables inline processing of surfaces and webs, the treatment of flowing gases or animals and humans. However, most of these plasmas are of transient nature, and the discharge duration is in the range of nano- to microseconds. Discharges in liquids are solely transient. Due to the omnipresent electrical conductivities of most liquids (water in particular) its pulsed operation is mandatory. The transient character and short duration as well as the erratic appearance and its small scale (micro- to millimeter range) are particular challenges for plasma diagnostics and modelling.

To develop new plasma sources and applications, and to control and optimize technologies it is mandatory to understand the fundamental processes and to gain quantitative knowledge on the basic plasma parameters such as the electron density or the electric field strength. The electric field value in plasmas is usually quantified in units V $m^{-1}$, as an electric field strength, or in Td (Townsends, a non-SI unit with 1 Td = $10^{-21}$ V $m^2$), as a reduced electric field strength $E/N$. The latter points out the scalability of the plasma properties with the gas number density. It was introduced in the second half of the 20th century as a temperature-independent alternative to the pressure scaled quantity of $E/p$ [3]. It is worth noting, that different communities in the low temperature plasma science use different variations of above mentioned units. In general, the barrier discharge community is usually connected to Td, while the streamer modelling and laser spectroscopy teams utilize kV $cm^{-1}$ for plasmas near atmospheric pressure. Similarly, the electron swarm parameters such as mobilities and ionization coefficients are dependent on $E/N$, so this community is also dominantly using the reduced electric field strength parameter in Td. However, the electron energy loss fraction in inelastic processes such as ionization and dissociation and thus, the electron energy distribution function (EEDF) and consequently, the rate coefficients are functions of $E/N$. Therefore, to control $E/N$ gives possibility to control the generation of reactive species and the ongoing plasma chemistry.

The purpose for this topical review is to provide a single, concise reference for non-invasive optical diagnostics for electric field strength measurements within the discharge itself. In particular, we will focus on both linear and non-linear diagnostics, each of which has its own unique advantages and disadvantages. This topical review will discuss: (i) optical emission spectroscopy (OES) based approaches, (ii) laser induced fluorescence dip (LIF-DIP) spectroscopy, (iii) E-field four wave mixing, and (iv) electric field induced second harmonic generation (E-FISH).

It needs to be mentioned that non-optical methods to measure the electric field strength has made a substantial contribution to the field. In principle, information about the electric field might be obtained from electrical measurements. However, precise voltage measurements are a challenge in case of transient plasmas, and, for fast-pulsed high voltage (HV) operation in particular due to not impedance-matched cables and thus, reflections of the HV pulse and/or limited bandwidth of the equipment. These difficulties can be mastered by D-dot and B-dot sensors, which are compactly mounted on the coaxial cable that connects a nanosecond pulse HV source to its load [4]. Another method for electric field—related measurements are capacitive probes. These detectors allow the measurement of the electrical potential distribution along the discharge gap with a mm-accuracy. They were applied to study the breakdown front in nanosecond discharges at lower pressure [5, 6]. The reader is referred to the cited literature to get more information about these approaches. However, it must be emphasized, that in many plasmas the (local) electric field strength cannot be directly derived from the voltage and the electrode geometry due to the distortion by volume and surface charges.

Several experimental techniques to measure the electric field inside solid substrates or electrodes were applied, too. This includes measurements on the target of plasma jets or the barrier of dielectric barrier discharges. In most cases, the substrate/barrier consist of bismuth silicon oxide (BSO), an electro-optic crystal. The local electric field induces birefringence resulting in rotation of polarization of incident light. The change of polarization is a measure for the electric field strength, which can be induced by plasma impact or the deposition of surface charges on non-conducting materials [7–11]. The dynamics and formation of discharge pattern was studied, e.g. in [12] and later applied to measure the surface charge during the breakdown, i.e. extended for phase-resolved or time resolved studies [13]. It must be noted, that BSO and other electro-optic crystals have a relatively large dielectric constant. Thus, the plasma properties in case of the crystal as the barrier/substrate can (but not necessarily must) differ from the one being obtained with common dielectric substrates (glass, ceramic, polymers, agar, …) or life matter. Meanwhile, the Pockels-effect method has been made accessible to various dielectrics to determine the dynamics and spatial distribution of surface charges on borosilicate glass, mono-crystalline alumina and magnesia [14]. These optically transparent materials covered the crystal in these experiments.

Recently, the use of electro-optic materials as a substrate was used to obtain the electric field induced by plasma jet impinging [15]. This work utilized Mueller polarimetry, i.e. by measuring the Mueller matrix of the electro-optic target. While electric fields are due to deposited surface charges, information about plasma induced temperatures can be obtained simultaneously due to the photo-elastic effect by this approach. The technique offers high sensitivity in the determination of the temperature variation and, the evolution of the electric field strength in the target can be measured with the threshold of the order of $10^5$ V $m^{-1}$ [16].

Using a small electro-optic crystal, fiber-like sensors were developed as well. Such probes allow to measure the electric field strength spatially and temporally resolved in plasma jets propagating inside dielectric tubes and thus, far ahead of the ionization front [17]. The above mentioned capacitive probes were utilized as well for indirect electric field determination [18, 19]. Since these methods characterizes the electric field in a somewhat indirect manner they are not included in this review and we refer to the cited literature.

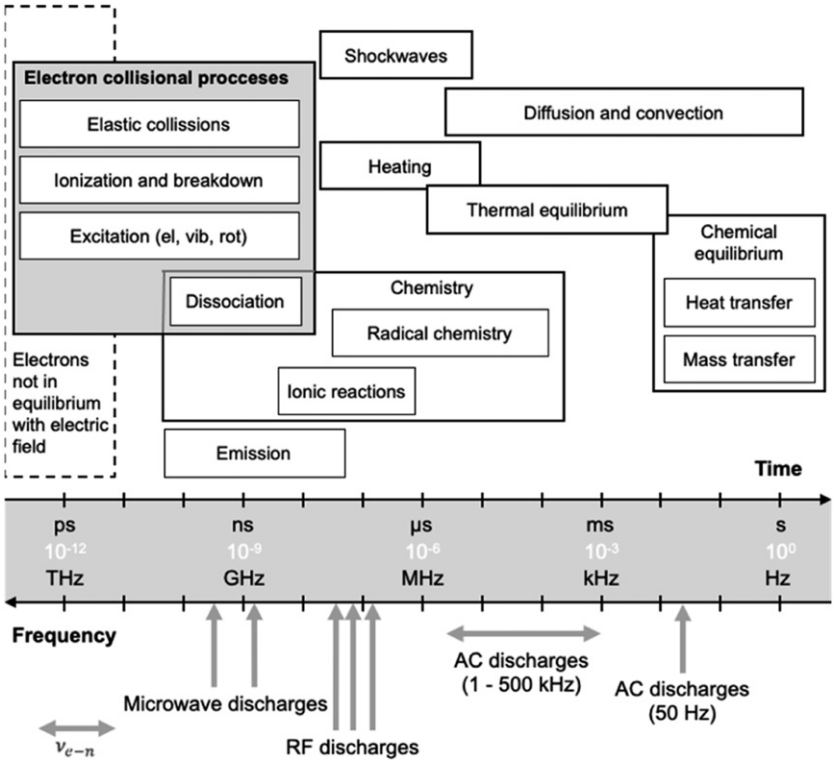


**Figure 1.** Typical timescales of relevant collisional and transport processes in atmospheric pressure plasmas related with applied HV operation frequencies.

## 2. Electric field and discharge time-scales

In non-equilibrium plasmas at elevated pressure the time scales for collisional processes and transport span over 12 orders of magnitude. The most important processes with their typical time scales are sketched in figure 1. The process time scales are related with a frequency scale to point out the relation with this operation parameter.

An important aspect is that electron collisional processes typically take place in picosecond time scales at elevated pressures or background medium densities. The large collisionality of atmospheric pressure discharges (see the marked range of electron-neutral collision frequency $\nu_{\text{e-n}} \sim$ THz in figure 1) also leads to short energy relaxation times [20–24]. These short times tend to drive the electron kinetics in equilibrium with the instantaneous electric field. Note that the local electric field is not essentially the applied electric field due to the distortion by local space charges. Nevertheless, for cases with high spatiotemporal electric field gradients a non-relaxed electron ensemble should be considered [25, 26]. The energy relaxation time is orders of magnitude smaller than typical periods of the applied voltage waveform, even for microwave sustained discharges (see the bottom part of figure 1). The EEDF relaxes typically in a few picoseconds in atmospheric pressure air [20, 21]. Discharge inception, dissociation reactions and wave-ionization processes proceed at hundreds of picoseconds and nanosecond time scales.

The highly frequent electron-neutral elastic collisions result in significant energy transfer to the background gas. Gas heating through elastic collisions, and, in the case of molecular gases, vibrational excitation typically takes between 100 ns and 1 $\mu$s. The recombination of highly excited atoms and molecules can also contribute to a faster gas heating, which can lead to creation of shock waves by sudden increases in pressure. The time scale for this process is in the range of 100 ns to $\mu$s. This also applies for the initiation of radical chemistry, ionic recombination reactions and dissociation processes (time scales form ns to $\mu$s). Neutral (radical) induced reactions are typically slower (microsecond to millisecond time scale). The coupling of transport through diffusion and convection takes typically between tens of $\mu$s up to several seconds [27]. Although the above-mentioned processes run at much larger time scales than needed for equilibrium formation between electrons and electric field, the knowledge about its dynamic and quantity is important for them, too. All rate coefficients $k_x$ of direct electron collision processes are determined by the EEDF which is a function of electron energy $\varepsilon$—for given reduced electric field $E/N$, and by the energy-dependent collision cross-section $\sigma_x(\varepsilon)$.

At this point it is worth emphasizing that the temporal development of the local electric field in the plasma is mostly not identical with the time scale of the applied voltage applied to the electrodes. As already mentioned, it is due to the accumulation of free charges in volume and on the surface, if dielectric material are present in the system. Local accumulation of free charges may result in charge separation with local electric field enhancement—initiating discharge mechanisms with characteristic times shorter than the externally applied electric field. Typically, such mechanisms include ionizing

waves (spatially symmetric—spherical or planar) or streamers (contracted ionizing waves and discharge channels) on the sub-nanosecond timescale. As a result, even a nanosecond description (experimental resolution or computational step in simulation) is not necessarily sufficient if pulsed discharges are investigated with HV rising slopes in the range of a few nanoseconds. Meaning, at some threshold of the HV waveform the streamer can be generated with dynamics on sub-nanosecond time scales. Due to the discharge contraction/filamentarization under some conditions (high-pressure, no pre-ionization etc), similar reasoning is valid also for spatial scales. Strong gradients of electric field strength or electron density can occur with significantly shorter dimensions than the interelectrode distance.

## 3. Electric field measurement methods

### *3.1. Optical emission based*

OES is a powerful technique for plasma diagnostics. There are numerous methods based on OES used for the determination of various plasma parameters: electron density, temperatures from rotational, vibrational or excitation quantum state distributions and, of course, electric field strength. The main advantage of the OES methods is their complete non-invasiveness, as they rely only on the light emitted by the plasma itself. For transient plasmas, the main challenge is to provide sufficient time resolution of the emission measurement. Here we will describe methods for direct measurements of the electric field using the Stark effect and methods for electric field strength determination using collision-radiative models. Both groups of methods have advantages, disadvantages, and limited applicability which we will discuss in close detail.

While the above-mentioned methods are certainly of broad usage, it is worth noting that other methods have been utilized for the electric field determination. For example, Navrátil *et al* [28] were able to identify weak neutral bremsstrahlung emission in barrier discharge during its dark phase and fitted such emission using the EEDF under action of searched electric field strength.

*3.1.1. OES methods based on collision radiative schemes.* The electric field strength can be determined using a collision-radiative model from the intensity ratio of two well-selected atomic lines or spectral bands. The time-independent intensity ratio methods for plasma diagnostics (electron density determination dominantly) were reviewed by Zhu and Pu [29]. In our case, the ratio, as the experimentally accessible parameter, has to be sensitive to the electric field strength. Such condition is fulfilled only if the radiative states responsible for the selected optical emission have significantly different excitation energy thresholds, and both radiative states are excited by direct electron impact. The intensity ratio serves as an indicator, which is weighting the relative contribution of the electrons with higher energy (responsible for population of the radiative state with higher excitation energy threshold) against the contribution of electrons with lower energy (responsible for population of the radiative state with lower excitation threshold). Dominant direct electron impact excitation implies that the line ratio reflects the energy of the electrons properly. Furthermore, the kinetic equation describing the radiative states will contain only one source term. The source term contains the rate coefficient of the excitation process being a sole function of the reduced electric field strength: $k_{\mathrm{exc}}(E/N)$. If stepwise excitation (e.g. due to the presence of metastable species, local pre-ionization etc) has to be considered, additional source terms must be considered as well which complicates the analysis (see for example [30, 31]). The energy of the exciting electrons is determined by the local electric field—the parameter we aim for.

The mentioned concept has meaning only if the radiative states are populated by the local electrons, i.e. electrons which gained their energy from the electric field at the same time and space coordinates. Non-local excitation via runaway electrons or other remote sources should be of negligible contribution in the investigated system. The spatiotemporal locality, i.e. the validity of the local field approximation, has to be checked for the particular experiment theoretically. This is needed especially if the electric field must be quantified with high spatiotemporal resolution. Such justification of the hydrodynamic approximation can be done, for example, by comparing the collision frequencies for momentum and energy dissipation as well as the mean free path and the energy dissipation length with the frequency and length of the electric field variation, respectively. More precisely, the spatial and temporal relaxation of the electron gas temperature in the expected electric field strength range can be investigated using Monte-Carlo simulation or solving the time dependent Boltzmann equation [20, 21, 32–35].

The approach described above is universal but best known for its applications on air plasmas. The method found its use in a broad area of science where the ionization of air takes place, besides the plasma-physical laboratories [33, 36, 37] also in investigations of transient luminous events in upper Earth atmosphere or plasma generation via extreme hydrodynamic shear [38–40]. In its limited steady-state (or time independent) form, the method has been applied since the 1970's by Gallimberti and others [41–43]. To our best knowledge, towards its time-dependent form, it was developed in the late 1990's [44–46] and utilized with high spatiotemporal resolution by Kozlov *et al* in 2001 [36]. It is worth noting that the time-independent form of the method results in an effective, averaged, value of the electric field strength parameter as it was shown in [47–51]. In the next paragraph, we describe the method for the air plasma case and discuss its general features for possible development of new forms of the method for other gas mixtures.

The radiative states $N_2(C_3\Pi_u)_{v'=0}$ and $N_2^+(B^2\Sigma_u^+)_{v'=0}$ considered for the method in the case of transient plasmas in air are responsible for the emission of the second positive (through transition to the $N_2(B_3\Pi_g)_{v''}$ state) and the first negative (transition to $N_2^+(X_3\Sigma_u^+)_{v''}$ state) spectral systems of molecular nitrogen. Although various combinations were discussed, we

will focus here on the $v'$-$v''$ = 0-0 vibrational transitions of these systems with spectral band heads at $\lambda_{C,0-0} = 337.1$ and $\lambda_{B,0-0} = 391.5$ nm, respectively. The direct electron impact excitation processes of these radiative states are described by the following two equations:

$$e + N_2\left(X^1\Sigma_g^+\right)_{v=0} \rightarrow N_2(C_3\Pi_u)_{v'=0} + e, \quad \Delta E = 11.0 \text{ eV}; \tag{1}$$

$$e + N_2\left(X_1\Sigma_g^+\right)_{v=0} \rightarrow N_2^+\left(B^2\Sigma_u^+\right)_{v'=0} + 2e, \quad \Delta E = 18.7 \text{ eV}. \tag{2}$$

The energy differences $\Delta E$ between the ground and the excited states are defining the necessary initial electron energy for a successful excitation by the direct electron impact. Note the relatively high difference (approximately factor of two) in the excitation thresholds as pointed out earlier. The electron excitation processes for population of $N_2(C_3\Pi_u)_{v'=0}$ and $N_2^+\left(B^2\Sigma_u^+\right)_{v'=0}$ states are defined by the rate coefficients $k_C(E/N)$ and $k_B(E/N)$, respectively. The equations describing the radiative quenching of the radiative states are accordingly:

$$N_2(C_3\Pi_u)_{v'=0} \rightarrow N_2\left(B_3\Pi_g\right)_{v''=0} + h\nu_{C,0-0}, \lambda_{C,0-0} = 337.1 \text{ nm}, \ \tau_{00}^C = 36.6 \text{ ns}, \tag{3}$$

$$N_2^+\left(B^2\Sigma_u^+\right)_{v'=0} \rightarrow N_2^+\left(X_3\Sigma_u^+\right)_{v''=0} + h\nu_{B,0-0}, \lambda_{B,0-0} = 391.5 \text{ nm}, \ \tau_{00}^B = 64.0 \text{ ns}, \tag{4}$$

where ${\tau_{00}}^C$ and ${\tau_{00}}^B$ denote the radiative lifetimes of the radiative states. The collisional quenching processes for the radiative states by nitrogen and oxygen molecules are:

$$N_2(C_3\Pi_u)_{v'=0} + N_2/O_2 \rightarrow \text{products}, \tag{5}$$

$$N_2^+\left(B^2\Sigma_u^+\right)_{v'=0} + N_2/O_2 \rightarrow \text{products}. \tag{6}$$

Both collisional and radiative quenching results in an effective quenching rates of ${\tau_{eff}}^C = 0.640$ ns and ${\tau_{eff}}^B = 0.045$ ns for the $N_2(C_3\Pi_u)_{v'=0}$ and $N_2{}^+(B^2\Sigma_u{}^+)_{v'=0}$ states in atmospheric pressure air, respectively. For more details see e.g. [52, 53] and further in the text.

The above-mentioned processes describe sufficiently accurate the kinetics concerning the two mentioned radiative states for its use for simple collision-radiative scheme in transient plasmas. It is important to note that the values of the radiative lifetimes or collisional quenching coefficients (and thus the effective lifetimes) and rate coefficients differs in the literature and their proper selection is a subject of discussion, see e.g. in [30, 52, 54–58] and further in the text. The scheme is sensitive enough for the electric field strength determination even in kHz frequency repetitive atmospheric pressure air transient plasmas. It was validated by means of sensitivity analysis approach by Obrusník *et al* [30], where these processes remain as the only dominant after a simplification of the full collision-radiative model for selected conditions.

Rewriting the described processes into balance equations for the radiative states density change we obtain the crucial

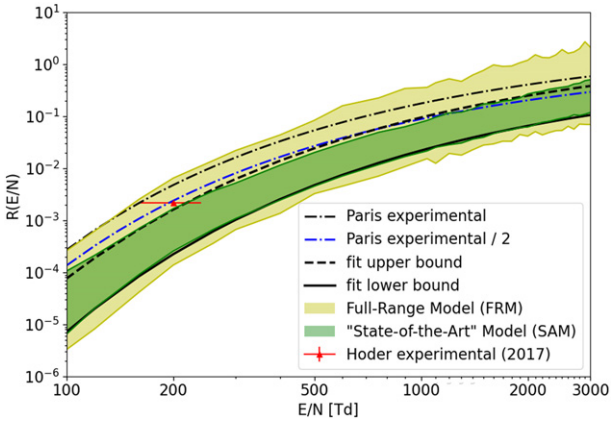


**Figure 2.** The dependence of the ratio $R_{FNS/SPS}(E/N)$ on the reduced electric field strength. Reproduced from [31]. The experimental dependence of Paris *et al* divided by two is included for comparison. 

building blocks:

$$\frac{dn_C(x,t)}{dt} = k_C\left(\frac{E}{N}\right) n_{N_2} n_e - \frac{n_C(x,t)}{\tau_{eff}^C}, \tag{7}$$

$$\frac{dn_B(x,t)}{dt} = k_B\left(\frac{E}{N}\right) n_{N_2} n_e - \frac{n_B(x,t)}{\tau_{eff}^B}. \tag{8}$$

Substituting the state densities with light emission intensities in the form of $I_C(x,t) = T_C n_C hc/({\tau_{00}}^C \lambda_{C,0-0})$ and $I_B(x,t) = T_B n_B hc/({\tau_{00}}^B \lambda_{B,0-0})$, dividing the two equations and after some rearrangements (see e.g. in Hoder *et al* [20]), we obtain the following equation:

$$\frac{\frac{dI_B(x,t)}{dt} + \frac{I_B(x,t)}{\tau_{eff}^B}}{\frac{dI_C(x,t)}{dt} + \frac{I_C(x,t)}{\tau_{eff}^C}} \cdot \frac{\tau_{eff}^B}{\tau_{eff}^C} = \frac{k_B\left(\frac{E}{N}(t)\right) T_B \tau_{00}^C \lambda_C \tau_{eff}^B}{k_C\left(\frac{E}{N}(t)\right) T_C \tau_{00}^B \lambda_B \tau_{eff}^C} = R_{\frac{FNS}{SPS}}\left(\frac{E}{N}(t)\right). \tag{9}$$

On the left side of equation (9) are known or measured quantities, described previously. The effective lifetime values are based on selective measurements of the quenching rates made by Dilecce *et al* [52] and are recommended also in [53]. In the middle is the electric field dependent ratio of rate coefficients for the underlying processes, $T_C$ and $T_B$ are the detection probabilities of photons of given wavelength (determined by the detector quantum efficiency and the transmission coefficients of the optical set-up). $T_C$ and $T_B$ can be determined by relative-intensity calibration. The radiative lifetimes are $\tau_{00}^{B,C}$. These parameters then give the so-called theoretical calibration curve for the ratio dependence on the electric field strength (see figure 2) which is changing in time $R_{\frac{FNS}{SPS}}(\frac{E}{N}(t))$, on the right side. The detected waveforms of the optical emissions are presented in figure 3(a) as well as the main components of the left side of the equation (9).

The determination of the accurate dependence $R_{FNS/SPS}(E/N)$ is the key point of the method and was treated by many researchers previously ([54–56], to name a few). If approached theoretically, the computation of the ratio of the reaction rates is the main task. We recommend a

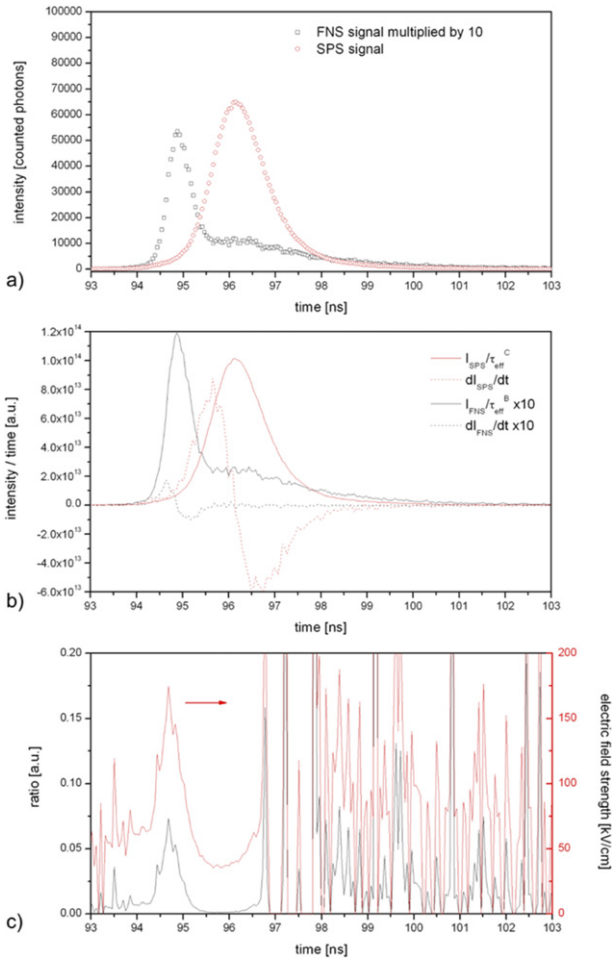


**Figure 3.** The high-resolution temporal development of the FNS and SPS signals in volume streamer propagating in coplanar barrier discharge in atmospheric pressure air (a). Evaluated terms from the equation (9), part (b), and the resulting ratio and electric field strength, part (c). The determination of the electric field from the ratio values takes into account the relative intensity calibration of the detector. Note that all FNS or derived waveforms are multiplied by ten to be in scale. Also, no smoothing or data fitting was used in the process. Reproduced from [61]. © IOP Publishing Ltd. All rights reserved.

modified form of the original dependence of Paris *et al* [54], but multiplied by factor of 0.5. This modification is based on comparison of the method with other approaches for *E*/*N* determination, as proposed in [53, 60–63]:

$$R_{\frac{\mathrm{FNS}}{\mathrm{SPS}}}\left(\frac{E}{N}\right) = 0.5 \cdot 46 \cdot 0.065 \cdot e^{-89\left(\frac{E}{N}\right)^{-0.5} - 402\left(\frac{E}{N}\right)^{-1.5}}, \quad (10)$$

where the reduced electric field strength is in Townsend units, 1 Td $= 10^{-21}$ Vm$^2$ (see also Paris *et al* [54]).

The uncertainty of the dependence of the ratio on electric field comes from a broad class of sources which were quantified by Obrusník *et al* [30] for air and Bílek *et al* [59] for nitrogen. The sources of the uncertainty may be the different Boltzmann equation solver, set of cross-sections for electron impact interaction [31], the quenching coefficients [52, 53, 57, 58], rotational temperature of the gas, if analyzed for short wavelength intervals [20] etc. The ratio dependence on the reduced electric field strength, as given by both the original and modified $R_{\mathrm{FNS/SPS}}(E/N)$ dependence of Paris *et al* is shown in figure 2, together with the results of the state-of-the-art model resulting from the uncertainty quantification and fundamental data selection as discussed in [59]. It is worth noting that the proper dependence is still discussed in the community.

The evaluation of the high-resolution data of the nitrogen spectral band intensities measured at a selected position in a single filament coplanar barrier discharge in air at atmospheric pressure can be followed in figure 3. The electric field of an early stage streamer is studied. In general, the time-dependent intensity ratio method finds its use in diagnostics of plasmas with fast ionizing waves or streamers. In the part (a) of figure 3, the measured data are shown. The time-correlated single-photon counting device with approx. 50 ps sampling was used [61]. The importance of the time-dependent kinetic scheme is well apparent from figure 3(b), where the temporal derivatives of the signal intensity waveforms are shown in comparison with the contribution of the signal intensities divided by the effective lifetimes, see the left side of equation (9). The derivative is for both cases significant; in the case of the SPS signal, it is comparable to the contribution of the steady-state term $I_{\mathrm{B}}(x,t)/\tau_{\mathrm{eff}}^{\mathrm{B}}$ itself. Apparently, for high temporal gradients of the measured intensity the contribution of the derivative to the resulting time-dependent intensity ratio may be even dominant. Note that all magnitudes in figure 3 related to the FNS signal are multiplied by 10 to be in scale. In the part (c), the ratio waveform $R_{\frac{\mathrm{FNS}}{\mathrm{SPS}}}(\frac{E}{N}(t))$ is shown as computed using the equation (9) (the left part of the equation) together with resulting electric field strength waveform according to the equation (10). The resulting electric field waveform is a re-computation of the ratio waveform (left side of the equation (9)) to the reduced electric field strength via the equation (10). It is worth noting, that the mutual delays between the electric field strength peak and the peak of FNS signal follow the theory as investigated in [50], i.e. the electric field maximum precedes the FNS peak by few hundreds of picoseconds. This duration also enables to evaluate the 2D streamer expansion during its propagation in free space [50]. Here nevertheless, the maximum of the SPS emission in figure 3(a) corresponds not to the head of the streamer, but to excitation by other discharge mechanisms later in its development.

The structure of the ratio and electric field strength development, as presented in figure 3(c), gives also the following information. The real electric field peak emerges from substantially higher noise around and precedes the FNS signal peak as discussed above. The noise level prior to this peak (i.e. prior 94 ns) is given by very low FNS signal amplitude in that phase of the discharge, ahead of the streamer head, where the local electric field strength is much lower. The increased noise signal behind the electric field peak (after 96.5 ns) is caused by transition of the discharge into other phases connected with, again, the low electric field strength values and, therefore, low FNS signal and the fact that the derivative of the SPS signal becomes relatively oscillating as well, from the same reasons. In addition, other interaction of radiative state molecules in already pre-ionized gas may distort the values of (mainly) SPS signal (see e.g. [30, 64]). It should be noted that, to illustrate

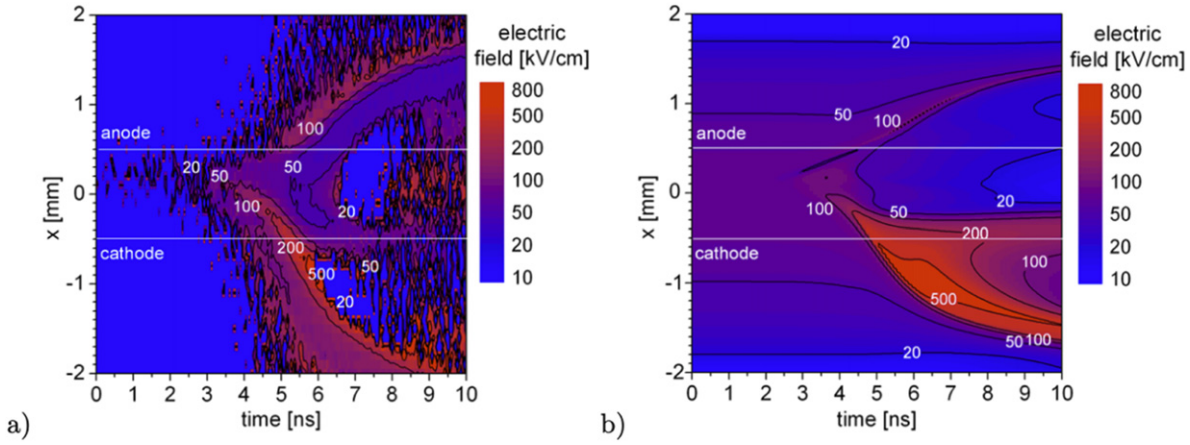


**Figure 4.** The electric field strength development as determined using the nitrogen molecular band intensity-ratio method for coplanar barrier discharge streamers in atmospheric pressure air (a). In the part (b), the results of the numerical simulation of the discharge phenomena in the same conditions are presented. Reproduced from [61]. 

the *E*/*N* determination process, the analysis presented here is done without any data smoothing procedure. An interesting fact is that in the later phases the ratio may become negative, if the negative differential term becomes larger than the signal intensity divided by the effective lifetime.

Regarding the temporal resolution limits, it is worth noting that in the case of time-dependent models the lifetime of radiative states poses no limitation. The equations (7) and (8) completely describe the development of the instantaneous state densities, where the lifetime is a parameter taken into account (see for example the discussion in [65] and for pure nitrogen [59]). With a detection device of sufficiently high temporal resolution (in the case of atmospheric pressure air discharges typically tens to hundreds of picoseconds, see [45, 46, 50]) the accurate quantification of temporal derivatives in equation (9) is possible and the time-resolution limiting factors are only the hydrodynamic conditions as mentioned above. The limitations of the method connected to temporal and spatial resolution for streamer diagnostics are obvious. Issues connected to the spatiotemporally averaged optical emission signal detection were subject of several investigations [29, 31, 32, 38–42, 59].

The electric field strength values determined by the intensity-ratio method can be confronted to other methods applicable under given conditions, for dielectric barrier discharges the Townsend coefficient fitting to the spatial profile of the SPS emission intensity may be applied [36, 37].

The above-mentioned intensity-ratio method was applied in its full time-dependent form to different kind of streamer or pulsed discharges. Its application to volume dielectric barrier discharge revealed the spatiotemporal electric field strength distribution with sub-nanosecond and sub-mm resolution using time-correlated single-photon counting for the first time [36]. Based on this result the authors also determined the ozone production rate on the same spatiotemporal scale. The authors also presented a two-dimensional *E*/*N* development with sub-nanosecond resolution [66]. Shcherbakov and colleagues applied this method to determination of the *E*/*N* development in streamer discharge in point-to-plane metal electrodes arrangement with profound theoretical, experimental and technical analysis of the whole *E*/*N* quantification process [65, 67, 68]. Theoretical analysis of the influence of the spatiotemporal non-uniformities of the streamer discharges onto the *E*/*N* determination using the intensity-ratio method was presented in [47–49]. The highly spatiotemporally resolved *E*/*N* development in the regular Trichel pulse discharge in atmospheric pressure air was achieved in [33] and confirmed the presence of the positive streamer discharge in close vicinity of the cathode and revealed its development on 100 $\mu$m spatial interval. *E*/*N* was determined also in ultrafast discharges generated by HV nanosecond pulses by means of picosecond intensified and gated charge-coupled device (ICCD) camera imaging [62, 69]. In [70, 75] the authors used time-dependent form yet did not succeed in reconstruction of the whole *E*/*N* pulse profile.

Recently, the determination of the *E*/*N* development in highly-transient plasmas was done for for positive and negative streamers in close vicint and in contact with dielectric. The method was applied in time-dependent form in [61, 73] for coplanar barrier discharge (see figure 4). For transient luminous events and their analogs in low pressure air [40, 53, 72], see example in figure 5. For positive and negative streamers in close vicinity and in contact with dielectrics the method was applied in time-dependent form e.g. in [61, 73]. The time-independent form of the method was used to obtain new insight into the discharge dynamics in plasmas for assisted combustion, flow control, see for example [51, 74, 76].

The intensity-ratio method was applied also to plasmas in other gas mixtures, also excluding nitrogen, i.e. utilizing different collision-radiative schemes for electric field or electron temperature determination, such as for argon, helium and mixtures [29, 77–81].

*3.1.2. Stark polarization emission spectroscopy.* Direct determination of electric field strengths in plasmas was employed on the Stark effect in atmospheric pressure plasmas

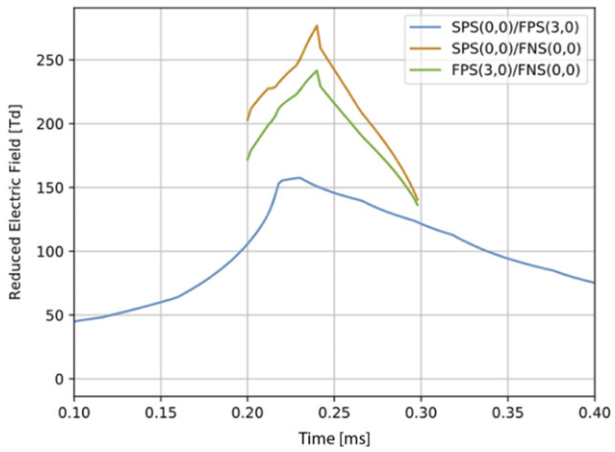


**Figure 5.** Temporal development of the reduced electric field strength in the halo transient luminous event using intensity ratio method from different spectral band intensities. [72] John Wiley & Sons. [©2018. American Geophysical Union. All Rights Reserved.]. The spectral emissions were recorded by ISUAL imager from FORMOSAT-2 satellite from space and presented in [38].

containing helium. In principle, the method of Stark polarization emission spectroscopy applies the polarization-dependent Stark splitting and shifting of atomic emission lines. Thus, it is exclusively limited to electric field measurements from plasma regions with emission.

The Stark effect describes the shifting and splitting of spectral lines of atoms/molecules caused by the presence of an external electric field. In spectroscopy, it is often observed as Stark broadening depending on the spectral resolution of the apparatus (instrumental broadening). The Stark effect enables the determination of electron density and electron temperature [82]. First measurements of electric field strength in the cathode fall region of glow discharges in hydrogen by Stark splitting was reported in 1919 [83] and several groups of authors have used polarization-dependent Stark splitting of hydrogen Balmer lines. In 1986, the first application on He I line splitting was reported [84]. In 1997, the application of the polarization-dependent Stark splitting and shifting of He I lines with relative wavelength shift measurements on a Grimm-type glow discharge at pressure 120–200 Pa succeeded [85].

To apply the method with spatial resolution the plasma emission is projected to the entrance slit of a spectrometer with a sufficient resolving power. The entrance slit width determines the spatial as well as the spectral resolution. A linear polarizer (plastic polarizer or Glan–Thomson prism), inserted between imaging optics and entrance slit, enables to collect either the axial or the radial polarized light and selects the spatial component of the electric field being investigated. An ICCD as the detector enables sensitive diagnostics with temporal resolution. The spatial resolution is determined by the CCD parameters and operation, e.g. pixel size and binning of pixels.

In helium the atomic line at 492.19 nm is often employed. In case of hydrogen the Balmer line $H_\beta$ at 486.13 is often used. It has to be checked, whether other spectral systems overlay the emission of interest. In this case, sophisticated line fitting procedures must be applied to improve the accuracy of wavelength calibration and electric field strength determination [86].

The displacement of energy sublevels in the external electric field can be evaluated by perturbation theory. The theoretical calculations by Foster were applied for higher levels of helium ($n = 4, 5$) and the linear Stark effect was obtained [67, 70]. From calculated displacements of the sublevels of allowed (A) line and its forbidden component (F) a mutual wavelength separation $\Delta\lambda$ of selected components (e.g. $\pi(\Delta m = 0)$ or $\sigma(\Delta m = +/-1)$ with $m$ as the magnetic quantum number) follows [85]. A detailed calculation for the different visible lines in helium and the discussion of its availability for the electric field strength determination can be found in [87]. The He I line at 492.19 nm (transition 2p $^1P^0$–4d $^1D^0$) and its forbidden component (2p $^1P^0$–4f $^1F^0$) is of particular interest because of its relatively strong emission intensity and high sensitivity to changes in electric field strength [86, 87]. The $\pi$-transitions are stronger and easier to measure for He I lines and are thus, applied in most of the studies found in literature. The wavelength shift $\Delta\lambda$ is dependent on the external electric field strength and fitted by polynomial functions ([85]) as follows.

$$\Delta\lambda_{FA} = C_1E^4 + C_2E^3 + C_3E^2 + C_4E + C_5.$$

Such polynomials are valid for a certain range of $E$. The range covered in [87] is up to 20 kV cm$^{-1}$ while the authors emphasize, that more complicated functions are required, or the dependence should be taken 'part by part' with different polynomial expressions in case of a wider range of electric field strength values. At low electric field strength the sublevel displacement by the quadratic Stark effect must be considered, but the calculated $\Delta\lambda$ from linear and quadratic theories coincide in the range 0.5–5 kV cm$^{-1}$. Above 5 kV cm$^{-1}$ the linear Stark theory is valid and it describes the displacement of all levels well, down to about 2 kV cm$^{-1}$.

The functional dependencies of the two components (F, A) on the local field strength can be used to determine its value from the measured peak-to-peak wavelength difference after applying a fitting procedure on the components shift. If the electric field strength is high enough to resolve the allowed and forbidden line (>1 kV cm$^{-1}$), its value can be directly obtained from the measured peak-to-peak wavelength distance $\Delta\lambda_{FA}$ according to the following equation.

$$E\left(\text{kV cm}^{-1}\right) = \left(-58.557 + 18.116\Delta\lambda_{FA} + 3130.960\Delta\lambda_{FA}^2 + 815.6\Delta\lambda_{FA}^3\right)^{0.5}.$$

For higher pressure, the accuracy is affected by line broadening as shown in figure 6. Part (b) shows the spectrum for a low pressure DC abnormal glow discharge at about 130 Pa [85]. The allowed and forbidden components can be distinguished clearly. A third line, the non-shifted or field-free (ff) component is detected also. Its intensity depends on discharge conditions and its origin is the emission of excited atoms which are outside the electric field region (and thus, inherent to the Stark effect), but still present in the optical path of the detection system. The electric field strength measured in the DC

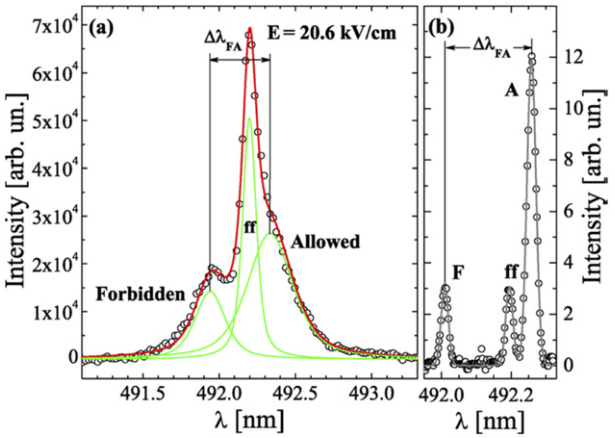


**Figure 6.** Typical $\pi$-polarized spectra of He I at 492.19 nm line recorded from (a) a helium plasma jet in air at atmospheric pressure [88] and (b) an abnormal DC discharge at low pressure [85]. F is the forbidden line, A is the allowed line, ff is the field-free component. Reprinted from [88], with the permission of AIP Publishing.

glow discharge is in the range of 7 to 17 kV cm$^{-1}$ in [85]. Part (a) in figure 6 is for a helium plasma jet at atmospheric pressure. The lines appear much broader and the ff-component marks the maximum of the overall spectral distribution. The allowed component can be separated only hardly from the ff-component and thus, a fitting procedure must be used which takes into account all transition components (including ff) in the vicinity of the allowed line, the instrumental function as well as the line broadening mechanisms (Doppler, van der Waals, pressure and resonant broadening) [87]. In the example in figure 6 the spectral lines are fitted with pseudo-Voight profiles and an essential part of the fitting procedure is the estimation of the ff-component. It overlaps with the allowed line and is van der Waals broadened. Finally, for the fitted profiles the wavelength difference gives a local electric field strength of 20.6 kV cm$^{-1}$ or about 90 Td [88]. The consideration of the line broadening mechanisms is of particular importance. Typically, Doppler broadening, and for high pressure discharges van der Waals broadening combined with resonant broadening fitting must be considered. The elements of the fitting function are then component profile functions being determined by the instrumental profile coupled with the possible broadening mechanisms. Beside pseudo-Voigt profiles, Gaussian or pure Voigt function may be obtained in experiments [87]. To separate Doppler broadening from Stark splitting is demonstrated in [89] for a hydrogen discharge at low pressure.

Stark polarization spectroscopy was also used to measure the electric field strength in diffuse barrier discharge in helium or helium/hydrogen mixtures as well as in helium plasma jets [86, 88, 90–93].

The use of the $H_\beta$ line Stark splitting for the measurement of the electric field strength in the cathode layer of a DC microplasma at atmospheric pressure in helium with admixture of hydrogen was also reported [94]. The electric field strength maximum of about 60 kV cm$^{-1}$ located at the cathode and the rapid decay over a distance of about 50 $\mu$m was in good agreement with a 1D, self-consistent model. The $H_\beta$ line is composed of seven allowed transitions (main quantum number from $n = 4$ to $n = 2$) while 20 experimentally observed Stark components shape the overall line profile [95]. In microplasmas being investigated in [94, 95] the Stark as well as the Doppler broadening are negligible in the cathode sheath region due to the local low particle density. Thus, the relevant broadening mechanisms for each component of the $H_\beta$ line are van der Waals and instrumental broadening. The profile results from the broadening and shift of all Stark components, which is described by an algebraic normalized pseudo-Voigt function.

The limitation of the method to helium and hydrogen atoms is not obvious since the Stark effect is not restricted to helium and hydrogen atoms. However, the application to other gases at higher pressures, e.g. argon is not possible since the allowed and forbidden (and broadened) lines cannot be distinguished at elevated pressures in such gases.

Another emission based method uses the intensity ratio of two helium singlet lines: He I $2^1$P–$3^1$D (at 667.8 nm) and He I $2^1$P–$3^1$S (at 728.1 nm) [96]. The correlation between the line intensity and the electric field is obtained via Stark polarization emission spectroscopy of the He I $2^1$P–$4^1$D line (at 492.19 nm, see above). Similar as described for air-plasmas above the method is based on the rate coefficient of excitation on *E*/*N*, but combines this with a calibration by Stark polarization spectroscopy (for He I $2^1$P–$4^1$D line at 492.19 nm, see above). By using the line ratio the electron density is eliminated from the source term in the kinetic equation. The calibrated line intensity ratio and its dependence on *E*/*N* can then be used for temporally resolved measurements. Singlet lines are used, because they originate dominantly from the ground state. Contrary, the emission of triplet lines of helium is affected by metastable species densities and, its analysis would require additional knowledge about this parameter. The feasibility of this method was demonstrated for the cathode region of a dielectric barrier discharge in helium at atmospheric pressure with time resolution better than 1 $\mu$s and a collisional-radiative model was utilized to confirm and obtain the functional dependence of the line ratio on the local *E*. Although this method is not independent of energy distributions and densities of plasma particles (contrary to Stark splitting and shifting) it can be useful for conditions resulting in a low intensity of the helium lines with its forbidden counterparts. Another advantage is the determination in low field strength regions where the Stark splitting method is limited due to the overlap of the atomic line and its forbidden component due to pressure broadening [97]. On the other hand, it is limited to high-pressure (e.g. atmospheric pressure) plasmas where the local field approximation is valid and for regions with a considerable electric field strength (>3 kV cm$^{-1}$) and a negligible contribution of metastable species to the excitation of helium atoms.

The Stark polarization emission spectroscopy and the line ratio methods appear rather simple, but, as already mentioned time resolution is mostly limited by the exposure time of the detection system. State of the art ICCD cameras with exposure times down to 0.2 ns are available, which

is more than sufficient for AC operated plasmas (e.g. diffuse dielectric barrier discharges) and RF discharges, but the electric field development cannot be followed in case of fast pulsed and/or transient plasmas if the breakdown proceeds in less than a ns and the discharge appearance jitters. Spectrally resolved streak cameras or time-correlated single photon counting provide sub-ns time resolution [98]. The stability or reproducibility of the discharges is a general concern since spectral profiles are mostly accumulated over several hundred to thousand events. To check the reproducibility, the plasma should be monitored by fast electrical measurements.

### 3.2. Laser based methods

*3.2.1. Laser induced fluorescence dip spectroscopy.* Laser induced fluorescence (LIF) was first observed in the late 1970's and has since become a well-known and used optical diagnostic for species concentration measurements in both reacting and non-reacting environments [99, 100]. In a typical LIF experiment, a laser tuned to an electronic excitation of the target molecule is focused either into a sheet (2D measurements) or a line (1D or point measurements). The excited species then radiatively decay into a lower energy state and the emitted radiation can be imaged using an intensified CCD camera or detected using a photomultiplier tube for enhanced sensitivity. LIF is well known for being an extremely sensitive measurement method, capable of species detection at parts per million concentration levels depending upon the specific experimental parameters.

While LIF has been used for more 'conventional' measurements since its inception in the late 1970's, a relatively recent alteration of the method has found utilization for extremely sensitive electric field measurements in low density atomic gasses [101–103]. The electric field variant is known as LIF-DIP spectroscopy and is based upon the Stark effect for shifting resonance frequencies. This method has been successfully utilized for 2D electric field imaging in low density transient plasmas with field sensitivities on the order of 1 V cm$^{-1}$. There have been numerous works and entire chapters dedicated to describing LIF and its variations and thus, will not be described here [104, 105]. Rather, we will focus on describing the LIF-DIP variant and how it is used for electric field measurements.

Figure 7 shows a cartoon energy level diagram for a typical LIF-DIP experiment. A target species is chosen in a specific energy level and then excited to a metastable electronic energy state, often through two-photon excitation. The electronically excited species then emits a photon to relax back to a lower energy level via radiative decay. In a typical LIF experiment, the radiative decay is the LIF signal of interest and can be monitored for species concentrations as well as temperature. For LIF-DIP, a second, tunable laser is used to resonantly excite the electronically excited species further from the metastable state into higher order Rydberg levels. When the species are resonantly excited into the Rydberg states, a 'dip' in the LIF signal is observed as a significant portion of the metastable population is transferred into the Rydberg state. Thus, by monitoring

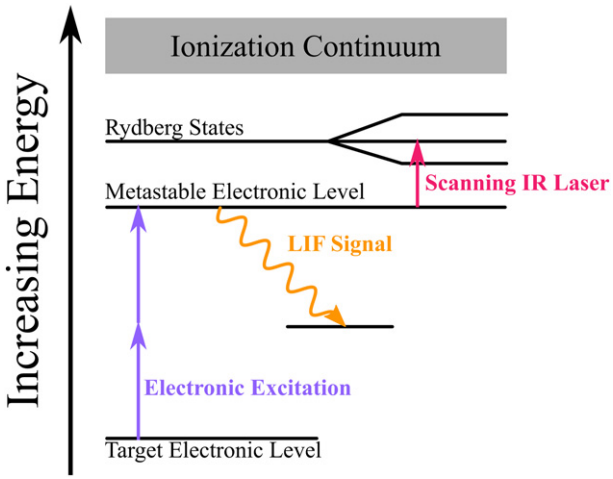


**Figure 7.** Energy level diagram for LIF-DIP spectroscopy.

when the dip occurs in the LIF signal as a function of the scanning laser frequency, one can determine the energy differences between the metastable and Rydberg states.

Without the presence of an electric field, the energy difference between the metastable and Rydberg states is known either through experiments or careful modelling of the target species. However, in the presence of an electric field, the higher order Rydberg states are Stark shifted where the magnitude of the shift is a function of the electric field. The electric field is then determined by comparing the change in magnitude of the Stark shifted dip frequencies with either experimental calibrations or advanced quantum mechanical models which predict the Stark shift of the target species [103, 106–111].

Due to the complexities of the system and the overall weak Stark effect, the method is only performed in atomic species such as hydrogen and the noble gasses [106, 109, 110, 112–114]. Furthermore, the method can only be performed in low density discharges to ensure that the Stark shifted dip is large enough to be measured against pressure broadening effects. One of the primary benefits of LIF-DIP is that it is extremely sensitive to small changes in the electric field and can used for 2D electric field maps with sub-millimeter resolution. Furthermore, the time resolution of the method is limited by the scanning laser duration and is typically on the order of several nanoseconds. For these reasons, LIF-DIP is most often used in low density discharges such as a DC glow or RF discharge where other laser based methods such as E-field CARS and E-FISH are unable to obtain sufficient signal.

A typical LIF-DIP experiments consist of two separate, synchronized lasers and a time gated intensified camera to monitor the LIF signal. The first laser is typically a tunable dye laser used for the two-photon electronic excitation step. The second laser is a then a scanning IR laser phase locked with the detection system (typically an ICCD for 2D imaging) and the voltage source frequency. The IR laser is then scanned and the spectral distribution of the Rydberg states is measured. The sensitivity of the method to changes in the electric field is limited by the target species and the IR laser linewidth, but can be on the order of $\sim$1 V cm$^{-1}$. The maximum electric field

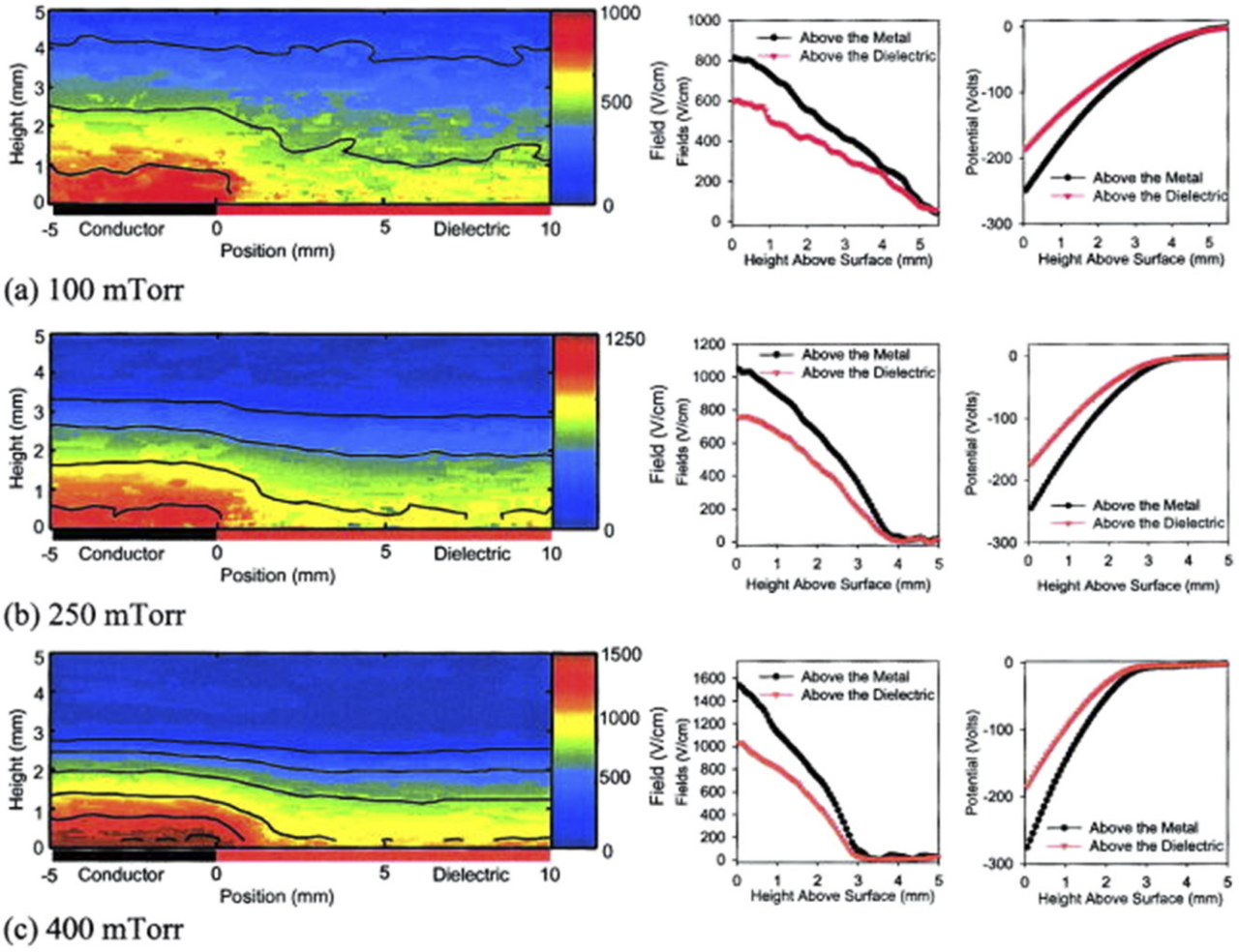


**Figure 8.** 2D electric field map at a metal-dielectric junction as a function of pressure. Measurements were carried out in an argon RF discharge driven at 320 $V_{pp}$ with a bias potential of $-120$ $V_{DC}$ . Reprinted from [117], with the permission of AIP Publishing.

strength which can be measured is typically on the order of 1 kV cm$^{-1}$, at which point there is often too much overlap between neighboring Stark shifted states.

While there had been previous work done observing Stark broadening of LIF signals [112, 115, 116], the first implementation of the method utilizing high order Rydberg states for enhanced sensitivity was demonstrated by Czarnetzki *et al* in [102] where atomic hydrogen was chosen as the target species. The researchers pumped ground state hydrogen into the $n = 3$ state and observed a constant fluorescence at the $H_\alpha$ line frequency ($\lambda = 656$ nm). A second IR laser was scanned over the Stark split resonance between the $n = 3$ state and higher order Rydberg states, observing a decay in the $H_\alpha$ emission as a function IR wavelength. The electric field strength was than measured by comparing the measured and calculated spectra. In that initial work, the researchers observed a broadening of the Rydberg states as a function of electric field and were able to deduce a linear relationship between the field strength and the experimentally measured linewidths. Furthermore, the researchers noted that the signal was sensitive to electric field vector components.

Following that original work, 2D electric field maps were first demonstrated by Czarnetzki *et al* in [108] where a grooved electrode was used to create a spatially varying electric field. At that time, the same excitation scheme was used and the discharge was sustained in 50 Pa of hydrogen atoms. The electric field was compared both with and without the presence of a dielectric barrier and each geometry was shown to be in good agreement with calculated predictions. Since then, 2D maps have become the preferred implementation of the method and are demonstrated in figure 8 where measurements were taken in an argon RF discharge focusing on the change in the electric field distribution formed around a metal-dielectric interface [117].

Having demonstrated the value of the method for sensitive 2D electric field measurements, much of the follow on work has focused on electric field measurements in the near wall sheath region of low density discharges. As computational models have evolved and excitation/detection methods have become more sensitive, larger atomic species have been studied. At present, measurements have been made in many of the noble gases such as argon [106, 107, 111, 113, 117, 118], Krypton [119, 120], as well as Xenon [109, 110].

*3.2.2. E-field CARS.* Coherent anti-Stokes Raman scattering (CARS) is a well known and widely practiced diagnostic

method for temperature and species concentration measurements in reacting and non-reacting flows [104, 121–123]. Typical CARS experiments are four-wave mixing processes where simultaneous pump and Stokes photons excite a ground state molecule into a higher ro-vibrational energy level depending upon the energy difference of the incident beams. A third photon, typically degenerate in frequency with the pump photons, inelastically scatters off the ro-vibrationally excited molecules generating the anti-Stokes signal photons. In a typical CARS experiment, the anti-Stokes beam is spectrally analyzed and fitted for temperature or species concentration measurements. CARS has been widely practiced for decades although is currently experiencing a renaissance of sorts with commercially available ultrafast laser sources now used for more efficient signal generation [122, 124], larger bandwidths for single shot measurements [125], and the capability to time delay the probe beam mitigating non-resonant background concerns which plagued earlier measurements [126]. Key benefits of the method are that temperature errors are typically on the order of 1% or less, the method can realize extremely high spatial resolution depending upon the phase matching configuration used, and that the signal beam is generated coherently allowing for efficient collection [104].

More recently, a similar method was developed for electric field measurements and is thus often described as E-field CARS [127, 128]. The E-field CARS process begins similarly as standard CARS where a pump and Stokes photon interact with the ground state molecules. However, in E-field CARS, the induced oscillation from the incident photons mixes with a net molecular dipole which acts as zero frequency probe beam. Due to the induced dipole, the molecular inversion symmetry is destroyed, allowing for the typically IR inactive molecules to radiate at their IR wavelength. The measured IR radiation scales with the square of the electric field and thus, the field in a transient discharge can be measured through careful calibration against a known electric field. Furthermore, similar to conventional CARS, the measured signal beam has a parallel polarization with the electric field allowing for field vector determination. Finally, the time resolution of the method is determined by the coherence decay time which is typically on the order of several hundred picoseconds for near atmospheric pressure discharges [129].

Figure 9 shows an energy level and phase matching diagram for both conventional CARS and the E-field CARS variant. It is readily seen that the E-field CARS method works analogously to conventional CARS and thus, we can follow the conventional CARS equations for growth to understand how the E-field CARS response is generated. While full classical and quantum mechanical derivations for the CARS equations for growth are readily available in text books [104], such a rigorous understanding is beyond the scope of the current topical review. It is sufficient to begin with an expression for the third order induced polarization which arises when the pump and Stokes beams interact with a Raman active molecule, expressed as:

$$P^{(3)}(\omega_{\mathrm{CARS}}, r) = \varepsilon_0 \chi^{(3)}_{\mathrm{CARS}} E^2(\omega_{\mathrm{Pump}}, r) \cdot E^*(\omega_{\mathrm{Stokes}}, r),$$

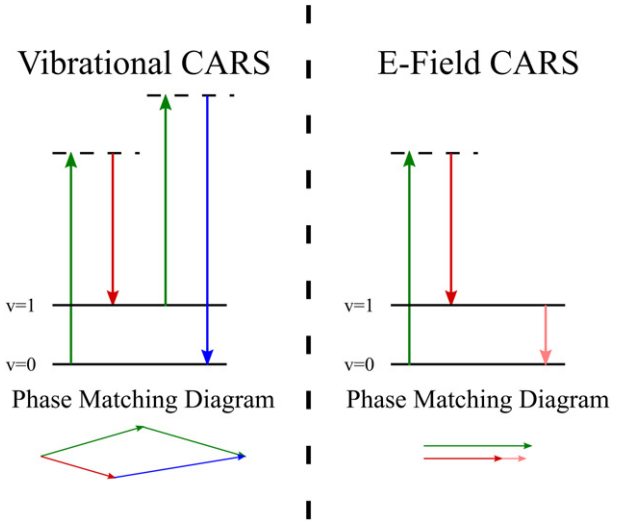


**Figure 9.** Vibrational and E-field CARS energy and phase matching diagrams. In both experiments, pump and Stokes photons interact with ground state molecules. In E-field CARS, the induced oscillation mixes with the external electric field allowing for the molecules to emit coherent radiation at their $Q(1)$ frequency.

where $P^{(3)}(\omega_{\mathrm{CARS}}, \vec{r})$ is the third order induced polarization at the CARS frequency, $\varepsilon_0$ is the permittivity of free space, $\chi^{(3)}_{\mathrm{CARS}}$ is the CARS susceptibility which is a molecule specific third order tensor, $E^2\left(\omega_{\mathrm{Pump}}, \vec{r}\right)$ is the electric field of the incident pump photons (note that the square is due to degenerate pump and probe frequencies), and $E^*(\omega_{\mathrm{Stokes}}, \vec{r})$ is the complex conjugate of the Stokes photon's electric field. Substituting a travelling wave expression for the lasers' electric field and reducing results in:

$$\begin{aligned} P^{(3)}(\omega_{\mathrm{CARS}}, r) = \varepsilon_0 \chi^{(3)}_{\mathrm{CARS}} E^2\left(\omega_{\mathrm{Pump}}\right) E\left(\omega_{\mathrm{Stokes}}\right) \\ * \exp\left[\mathrm{i}\left(2k_{\mathrm{Pump}} - k_{\mathrm{Stokes}}\right) \cdot r\right] \\ * \exp\left[-\mathrm{i}\left(2\omega_{\mathrm{Pump}} - \omega_{\mathrm{Stokes}}\right)\right], \end{aligned}$$

where $k_{\mathrm{Pump}}$ & $k_{\mathrm{Stokes}}$ represent the wave vector of the pump and Stokes beams respectively. Once again, we note that the factor of 2 in front of $k_{\mathrm{Pump}}$ is due to the assumption of degenerate pump and probe beam photons. The induced polarization can be substituted into the wave equation $(\nabla^2 E - \frac{1}{c^2}\frac{\partial^2 E}{\partial t^2} = \mu_0 \frac{\partial^2 P}{\partial t^2}$, where $E$ is the electric field vector, $P$ is the induced polarization within the medium, $c$ represents the speed of light and $\mu_0$ is the permeability of free space). Following the slowly varying wave approximation results in:

$$\begin{aligned} E_{\mathrm{CARS}} = \frac{\omega_{\mathrm{CARS}}}{2c \cdot n_{\mathrm{CARS}}} \chi_{\mathrm{CARS}} E^2_{\mathrm{Pump}} E^*_{\mathrm{Stokes}} \\ \cdot \frac{(\exp(\mathrm{i}\Delta k L) - 1)}{\Delta k}, \end{aligned}$$

where $n_{\mathrm{CARS}}$ is the population difference between the lower and excited states, $\Delta k = 2k_{\mathrm{Pump}} - k_{\mathrm{Stokes}} - k_{\mathrm{CARS}}$ is known as the wave vector mismatch, and $L$ is the interaction length for the signal generation process. In a standard CARS experiment, this interaction length is determined by the experimental setup

used and can be sub-millimeter if desired. However, for the E-field CARS variant, the interaction length is determined by the wave vector mismatch and is typically given as the coherence length which can be on the order of 10 centimeters.

The time averaged beam intensity is related to the square of the electric field. Thus, for the typical CARS generation process, the measured intensity is of the form

$$I_{\mathrm{CARS}} \propto |\chi^{(3)}_{\mathrm{CARS}}|L^2 \cdot I^2_{\mathrm{Pump}} I_{\mathrm{Stokes}} \,\mathrm{sinc}^2\left(\frac{\Delta kL}{2}\right). \tag{11}$$

As mentioned previously, the E-field CARS variant can be understood analogously to the standard CARS equations for growth. The key difference is that the probe beam is replaced with a 0-frequency external electric field. The local electric field induces a dipole in the medium, allowing the typically IR inactive molecules to emit coherent radiation at the $Q(0)$ Raman frequency when resonantly excited by the pump/Stokes photon pair. Thus, without repeating the derivation, the E-field CARS IR signal intensity is given by

$$I_{\mathrm{IR}} \propto |\chi^{(3)}_{\mathrm{IR}}|L^2 \cdot I_{\mathrm{Pump}} I_{\mathrm{Stokes}} |E_{\mathrm{Ext}}|^2 \,\mathrm{sinc}^2\left(\frac{\Delta kL}{2}\right), \tag{12}$$

where $I_{\mathrm{IR}}$ is the intensity of the signal beam, $\chi^{(3)}_{\mathrm{IR}}$ is the species dependent nonlinear susceptibility for the E-field CARS process, and $E_{\mathrm{Ext}}$ is the external electric field which is to be measured. Once again, $\Delta k$ is the wave vector mismatch given as $\Delta k = k_{\mathrm{Pump}} - k_{\mathrm{Stokes}} - k_{\mathrm{IR}}$ for the E-field CARS variant.

From this expression for the signal beam intensity, several important scaling parameters are immediately evident. The first is that the signal scales with the CARS susceptibility, which is a species specific term dependent upon the Raman cross section of the constituent gas medium. Thus, the method only works for Raman active molecules and works best for species with large Raman cross sections. To date, the method has only been used in $H_2$ ($\Delta\omega_{\mathrm{Raman}} = 4160\ \mathrm{cm}^{-1}, \sigma = 7.94 \times 10^{-30}\ \mathrm{cm}^2\ \mathrm{sr}^{-1}$) and $N_2$ ($\Delta\omega_{\mathrm{Raman}} = 2330\ \mathrm{cm}^{-1}, \sigma = 3.31 \times 10^{-30}\ \mathrm{cm}^2\ \mathrm{sr}^{-1}$) containing discharges [130–133]. Second, we note that the signal scales as the product of the intensities of the incident pump/Stokes beams with the square of the electric field. Thus, it is desirable to use high intensity, pico- and femto-second pulses rather than higher energy nanosecond pulses. Additionally, due to the electric field dependence, the method is well suited to measure large electric fields such as those present during the onset of breakdown in atmospheric pressure discharges. Finally, we note that the argument in the $\mathrm{sinc}^2$ function determines that the signal is optimized when $\Delta k = 0$, although this is never fully realized in practice due to the dispersive nature of gasses [133].

At present, nearly all work done with the E-field CARS method has used the second harmonic from an Nd:YAG laser system as pump beam. The Stokes beam frequency is then determined such that the frequency difference between the pump/Stokes pair matches the energy difference between the ground and first vibrational level energy difference for the species of interest. While results have been obtained in $N_2$ containing discharges, $H_2$ has been the far more popular choice due to the larger Raman cross section ($\sigma_{H_2} \approx 2.4 \cdot \sigma_{N_2}$) [104]. The Stokes beam is then generated either using a commercial dye laser [128, 134] or can be generated using a high pressure stimulated Raman shifting cell [135]. While the Raman shifting cell presents a significant simplification of the overall experiment, it is typically only used with picosecond lasers due to the higher energy conversion with shorter pulse lengths as well as the naturally broader bandwidth beams allowing for better spectral overlap between the pressure shifted Stokes beam and the first vibrational energy levels in the typically lower pressure discharge region [135–138].

When a dye laser is used, the individual pump and Stokes beams must go through separate time of flight delay lines to ensure that both beams arrive simultaneously at the measurement region [134]. When the Raman shifting cell is used, the time delay between the two beams is assumed to be negligible and both beams are simultaneously routed to the measurement volume using broadband mirrors. Regardless of how the Stokes beam is generated, the pump/Stokes pair must be collinear due to the phase matching conditions [133]. The collinear beams are then focused into the measurement region and recollimated using a matched, IR transmissive lens. Due to the similarity between the two methods, a vibrational CARS beam is also generated at the measurement region and can be used to enhance the signal to noise and account for shot-to-shot variations in the overall IR signal level.

The three visible beams (pump, Stokes, & vibrational CARS) are spectrally separated from the IR signal beam. Depending on signal strengths, the pump and CARS beams can then be measured on a standard photodiode while the IR signal beam is measured on an IR active photosensor such as an InSb or HgCdTe detector. When all three beams are measured, the electric field is determined by taking the ratios of equations (11) and (12), resulting in

$$\frac{I_{\mathrm{IR}}}{I_{\mathrm{CARS}}} \propto \frac{|\chi^{(3)}_{\mathrm{IR}}|^2}{|\chi^{(3)}_{\mathrm{CARS}}|^2} \frac{|E_{\mathrm{Ext}}|^2}{I_{\mathrm{Pump}}}.$$

This formula can be rearranged and solved for the electric field, resulting in

$$|E_{\mathrm{Ext}}| = A \cdot \sqrt{\frac{I_{\mathrm{IR}} I_{\mathrm{Pump}}}{I_{\mathrm{CARS}}}},$$

where $A$ is an experimentally determined calibration constant. Thus, by careful calibration against a sub-breakdown field, one can determine the transient electric field in the discharge.

When nanosecond lasers are used, the time response of the method is often the duration of the laser beams and thus, corresponds directly with when the laser pulse arrives with respect to the onset of breakdown [132]. This allows for signal averaging on an oscilloscope enhancing overall signal to noise ratios and data collection speeds. When picosecond lasers are used, the time response of the method is instead determined by the coherence decay time, typically dominated by collisional dephasing and is on the order of 100's of picoseconds at moderate pressures, enabling sub-nanosecond resolution given a sufficient oscilloscope sampling rate.

The E-field CARS measurement method was first demonstrated by Gavrilenko *et al* in 1992, where the second harmonic

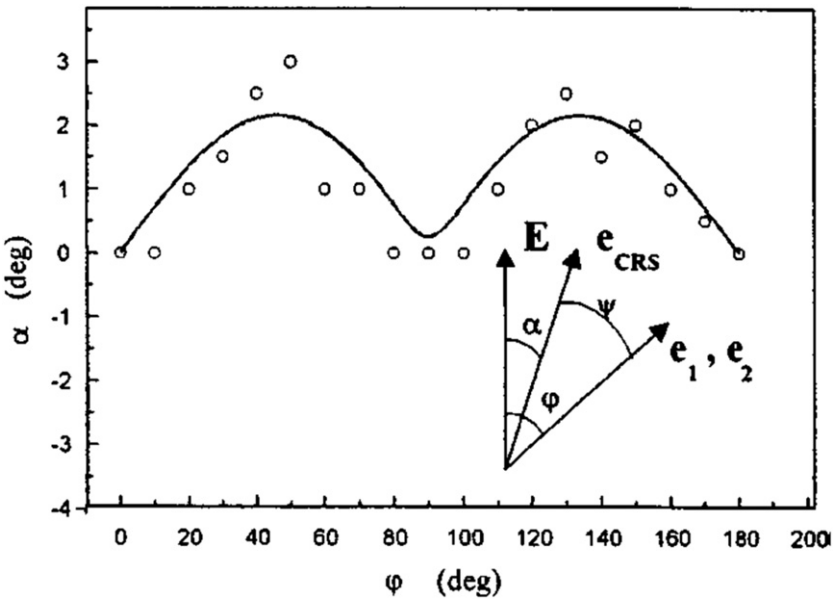


**Figure 10.** E-field CARS response with respect to the angle between the pump/Stokes polarization vector and the applied electric field. Reproduced from [141], with permission from Springer Nature. Experiments performed in 1.2 atm pure $H_2$ with an Nd:YAG pumped dye laser for pump/Stokes generation.

of a 10 ns Nd:YAG laser was used as a pump beam and a tunable dye laser was used to generate the Stokes shifted beam for the $H_2$ medium [139]. In that original work, the authors generated the E-field signal response at pressures up to 10 Bar while varying the electric field from 0–35 kV $cm^{-1}$ verifying the quadratic dependence of the measured signal intensity upon the applied electric field. Shortly thereafter, the same research group furthered their study on the effect, considering the measured signal upon experimental parameters such as pump laser linewidth and the phase matching requirements at higher pressures [140]. Even in that early work, the authors foresaw the technique's ability for electric field measurements in transient discharges by taking radial electric field measurements of a corona discharge sustained in $H_2$.

The sensitivity to electric field vectors was first demonstrated by Akimov *et al* in [141] when the authors varied the orientation of the pump/Stokes laser beams with respect to the applied electric field. Their results, shown in figure 10, demonstrated that the signal is essentially parallel ($\pm 3^\circ$) to the applied field and optimized when the pump/Stokes pair are parallel with the field as well. This would go on to inform future results where the method was used for field vector measurements in various electric fields. In a follow up work, the same research group used the method for time resolved electric field vector component measurements in a sliding arc discharge [142].

The first demonstration of the method for measurements in $N_2$ gas was completed by Lempert *et al* [128] where the dependence of the signal strength upon the field was verified in pure $N_2$ from 1.0–2.5 atm as well as in an open air environment. In this work, the [128] sensitivity limits of the method in $N_2$ were explored and the authors approximated that the IR signal response is a factor of $\sim 10^{-8}$ weaker than that of standard vibrational CARS, highlighting the need for intense laser pulses and extremely sensitive detection equipment.

The first application of the method for electric field measurements in near atmospheric pressure $H_2$ at time scales relevant to plasma formation was completed by Ito *et al* [131] where the electric field was measured in a repetitively pulsed nanosecond discharge and the results were compared against high speed imaging. The authors observed the presence of an ionization wavefront in the highspeed imaging and attributed the deviation between the measured electric field values and the nominal voltage to gap ratio to be due to the accumulation of space charge present within the discharge. In this work, the authors used a 3–5 ns laser pulse for signal generation, and thus were limited in the transient dynamics observable. Regardless, the results within provided much of the motivation for future studies utilizing ultrashort pulsed lasers as well as the push for measurements in $N_2$ containing discharges.

Picosecond lasers and the stimulated Raman shifting cell were first introduced by Goldberg *et al* [135], greatly simplifying the experimental setup and allowing for sub-nanosecond response. The electric field measurements were completed in a near atmospheric pressure dielectric barrier discharge and compared against kinetic modeling results and found to be in satisfactory agreement (see figure 11). The authors then went on to use the method for field vector resolved measurements of a surface ionization wave as well as to monitor the effect of nanosecond pulses upon the breakdown dynamics of AC DBD's [136, 143].

Up to this point, all measurements using the method in a discharge had been completed using $H_2$ due to the significantly larger Raman cross section. The first measurements in a mostly $N_2$ discharge environment were carried out in by Böhm *et al* [134] where a 10% $H_2$ admixture was included in a 1 atm $N_2$ discharge chamber, allowing for the first electric field measurements in an $N_2$ containing discharge. This work was followed upon in [132] where the method was converted to use

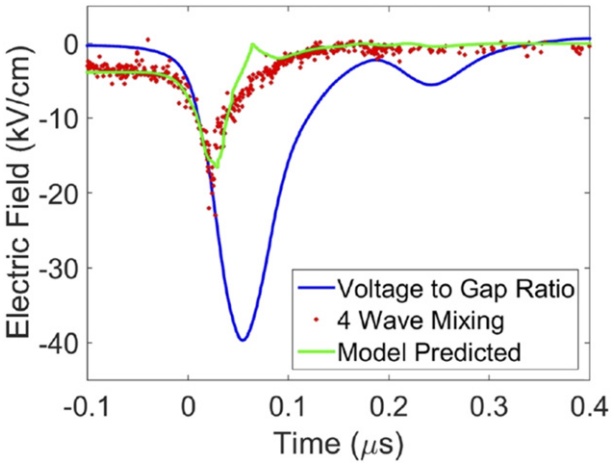


**Figure 11.** Electric field measurements sustained in a double dielectric barrier discharge presented along with the applied voltage to gap ratio and kinetic modelling predictions. Reproduced from [135]. © IOP Publishing Ltd. All rights reserved.

in open air by using $N_2$ as the target molecule rather than the $H_2$ admixture.

Simultaneously, work was ongoing using the picosecond laser and Raman shifting cell for measurements in $N_2$ containing discharges [133]. The true flexibility of the method was demonstrated by Simeni-Simeni *et al* in the follow up papers where the method was used for measurements over a liquid surface and in a hydrogen diffusion flame [137, 144].

Most recently, the measurement method has mostly fallen out of favor due to the relatively complex setup and poor spatial resolution. Due to the requirement of collinear beams, the resolution of the method is determined by the phase vector mismatch, which is on the order of 10 cm for measurements in $N_2$ [133]. While one could likely envision an unstable-resonator spatially enhanced detection system similar to that of CARS [145, 146], this has not yet been attempted to this point.

*3.2.3. E-FISH.* The E-FISH method represents arguably the current state of the art for laser based transient electric field measurements. In comparison to the E-field CARS method, E-FISH is an exceedingly simple experimental design and is known to work in any gaseous species as well as with many commonly available laser systems. The time response of the method is determined entirely by the pump laser pulse duration, allowing for pico- and even femtosecond resolution (although, in practice this is typically limited by detection sampling responses such as oscilloscope and photodiode response times). Furthermore, similar to the E-field CARS technique, E-FISH is capable of field vector measurements allowing for a complete determination of the plasma environment. Despite these benefits, the method is still prone to several experimental errors and one must be judicious in how they setup and control their experiment in order to obtain the highest fidelity measurements.

Although using the E-FISH effect for measurements of arbitrary electrical fields is a relatively recent idea, the effect itself has been known about and used for decades. The earliest theoretical works in understanding the E-FISH method date back to the early 1960's, where the advent of the laser allowed for large enough light intensities such that second harmonic generation could be observed [147, 148]. The method was first experimentally investigated in 1971 [149] and has since been used consistently over the years to measure third order nonlinear susceptibilities $\chi^{(3)}(\omega:\omega,\omega,\omega)$ [147, 150–154]. The technique was first suggested as a method for arbitrary electric field measurements in 2017 and first used for measurements in a plasma the following year [155, 156]. In the few years since its introduction to the plasma community, numerous papers have now been written about it from research groups all over the globe.

While full quantum mechanical derivations of the effect are available, it is beyond the scope of this review to go into such detail. Instead, we focus on the signal growth analogous to that in a nonlinear medium.

Second harmonic generation in a centrosymmetric system (i.e.—one *with* an inversion symmetry) is not possible. This includes many common plasma feed gases such as air, argon, and helium. However, when an external electric field is present, a net dipole is induced in the system, destroying the inversion symmetry. When such a system is acted upon by an intense laser light pulse, the incident photons interact with the induced dipole allowing for coherent growth of radiation at the second harmonic frequency of the pump source.

E-FISH is described as a third-order nonlinear process where two pump beam photons mix with the induced dipole, resulting in an induced oscillating polarization at the second harmonic frequency given by [153, 155]:

$$P_i^{(2\omega)} = \frac{3}{2} N \chi^{(3)}_{i,j,k,l}(-2\omega, 0, \omega, \omega) E_j^{(\mathrm{F})} E_k^{(\omega)} E_l^{(\omega)},$$

where $P_i^{(2\omega)}$ is the induced polarization at the second harmonic frequency $2\omega$, $E_{k,l}^{(\omega)}$ are the electric field of the incident laser, $E_j^{(\mathrm{F})}$ is the applied electric field to be measured, $N$ is the neutral species number density, and $\chi^{(3)}_{i,j,k,l}$ is the species and polarization dependent nonlinear susceptibility. The measured signal intensity is proportional to the product of $\left[P_i^{(2\omega)}\right]^2$, the interaction length, and a phase matching factor. Thus, the intensity of the second harmonic signal is given by [144]:

$$I^{(2\omega)} \propto [P_i^{(2\omega)}]^2 \cdot L^2 \cdot \left[\mathrm{sinc}^2\left(\frac{\Delta k L}{2}\right)\right],$$

where $L$ is the interaction length between the pump beam and the extent of the electric field and $\Delta k$ is the wavevector mismatch. When the interaction length, wavevector mismatch, and dominant species present can be controlled, the resulting signal intensity is often simplified to [156]:

$$I^{(2\omega)} = A \cdot N^2 (E_{\mathrm{Ext}})^2 (I_{\mathrm{Pump}})^2,$$

where $A$ is a measured calibration constant, $E_{\mathrm{Ext}}$ is the external electric field to be measured, and $I_{\mathrm{Pump}}$ is the measured intensity of the pump beam.

Figure 12 shows a typical experimental schematic for an E-FISH measurement. Often, an ultra-short pulse femto- or picosecond laser system is used to pump the system

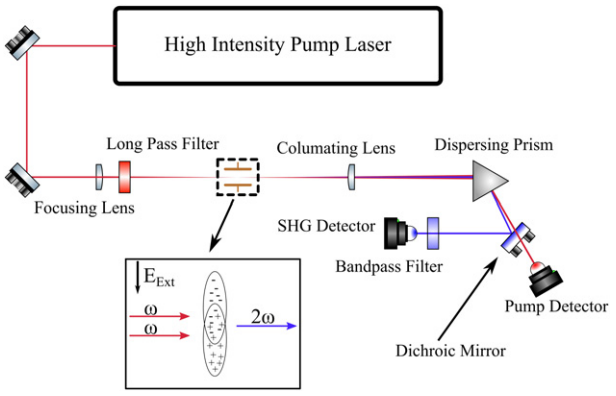


**Figure 12.** Typical schematic of an E-FISH experiment. A high intensity pump laser beam is focused into a region of interest where the electric field to be measured is present. The collinear pump and signal beams are then collimated and spectrally separated where each by intensity is measured.

[156–158]. This is due to the better time response as well as greater signal intensity possible. However, recent experiments using nanosecond lasers have demonstrated that the method is still effective despite the significantly longer pulse durations. The pump beam is then routed into the discharge region where it is focused either using a spherical lens for point measurements or a cylindrical lens for 1D imaging capabilities [159, 160]. Typically, the final optic the beam should traverse through is a long pass filter to remove any second harmonic light generated upon upstream reflective surfaces. The focused beam then travels through the measurement volume where it mixes with the electric field induced dipole and the second harmonic signal beam is generated. Both beams are then collimated and spectrally separated using a combination of dispersion prisms, dichroic mirrors, and/or bandpass filters. One important note is that grating based methods do not work well on their own for spectral separation due to the second order pump beam reflection being exactly coincident with the desired second harmonic signal. Finally, both the second harmonic signal and pump beam intensity are independently measured using some combination of photodiodes, photomultiplier tubes, and/or cameras and are then time correlated on a digital oscilloscope.

As mentioned previously, the physics behind the E-FISH method have been known and used for decades but the method itself has only recently begun to emerge as a tool for arbitrary electric field measurements. This idea was first proposed by Dogariu *et al* in reference [155] published in 2017, within which there were several key advantages the authors discussed. Primarily, the authors demonstrated that: (i) the method worked for all tested gaseous species, (ii) the signal strength scales with the polarization, (iii) the temporal resolution was determined by the oscilloscope rather than a fundamental physical process, and (iv) that the spatial resolution was determined by the beam focusing parameters. Since that initial work, (i)–(iii) have since been consistently used for electric field measurements while (iv) has recently come into question due to beam focusing parameters [161].

The method was first demonstrated in a nanosecond pulse discharge in by Goldberg *et al* [156] where argon was chosen as the process gas due to the spectral isolation of the second harmonic signal beam from the plasma induced emission. Furthermore, that work demonstrated the first time that a picosecond laser was used rather than a femtosecond, helping to make the method more readily applicable without the upfront investment of an amplified femtosecond laser. Shortly thereafter, the method was used for electric field vector resolved measurements of surface ionization waves in both positive and negative applied voltage pulse polarity configurations [144]. In that work, electric field vector measurements were compared against fast gated ICCD imaging to compare the effects of residual surface charge and voltage pulse polarity upon breakdown and ionization wave development.

While these initial works were only the first demonstrations of the E-FISH method, they combine to represent a clear direction that the research has now followed. For nearly all E-FISH measurements within a plasma, key focus has been on ionization wave propagation, where the innate high temporal resolution determined by the laser pulse allows insights into the required sub-nanosecond time scales required. Furthermore, the measurements are typically carried out in diffuse, high pressure discharges. It is important that the measurement region is uniform and diffuse as the method is inherently line of site integrated and as such large field regions within the plasma could significantly influence the measurement results.

Since then, there have been numerous interesting publications utilizing the E-FISH method. The method was first used for electric field measurements in a combustion environment by Simeni-Simeni *et al* [158], demonstrating the unique adaptability of the method compared to other nonlinear field measurement techniques. In order to accurately calibrate the technique, the authors opted to apply a sub-breakdown electric field in the flame itself, allowing for accurate calibration given a consistent temperature and combustion reaction products. It was shortly taken a step further by Retter and Elliott [157] when it was coupled with CARS, a well-known combustion diagnostic for temperature and species concentrations measurements [104, 122]. In that work, a single femtosecond laser was used both to generate the second harmonic measurements as well as a pump beam for the pure-rotational CARS experiment and the authors were able to account for shot-to-shot local species concentration and temperature variations by monitoring the CARS signal beam and thus were able to adjust the local hyperpolarizability as an enhanced calibration factor.

Further enhancements for the method have been completed by utilizing nanosecond lasers rather than the typical pico- and femtosecond pulses. This has made the method significantly more cost effective as many labs across the world now have readily available systems. A nanosecond laser system was first used by Cui *et al* [162], where the researchers observed that the steady state electric field under negative DC corona discharges varies from the peak onset field proportionally with the corona current density, calling into question the assumption that the field at the surface of the conductor remains constant at its onset value.

One of the primary issues with using nanosecond lasers for electric field measurements is that laser pulse duration is often

on the same order of magnitude of the underlying physics of interest. To this end, several interesting methods have been suggested as possible workarounds. One such method is to simply 'chop' the pulse using a Pockels cell powered by a sub-nanosecond voltage pulse source [163, 164]. Using this method, the lower intensity wings of the nominally Gaussian laser pulse can be suppressed, significantly decreasing the laser pulse duration allowing for enhanced temporal resolution. Of course, this comes with a decrease in laser pulse energy, but this effect is often found to be negligible in overall measured signals as pulse energy is rarely the limiting factor in signal generation.

A second proposed method for enhanced time resolution is to use the measured E-FISH signal response from the photomultiplier tube detector and compare it with the time domain photodiode response of the pump laser signal to verify a duration of time during which the signal is approximately constant [165]. This gives a temporal window over which one can claim that changes in the E-FISH signal response are due to electric field changes rather than pump laser intensity changes. This method is an attractive solution as it does not require any further equipment than what is currently in present for the standard experiment. We note that a more formal variation of this would be to use an ultrafast laser pulse as a $\delta$-function to measure the time response of the detection equipment (both PMT and pump beam photodiode) which can then be deconvolved from the measured signal response, allowing for a more consistent method over which changes in the measured signal are due exclusively to changes in the field.

Much of the E-FISH work completed to this point is for time resolved measurements of ionization waves [166–168]. In fact, this is even true of the first E-FISH measurements in a discharge, where the field measured exceeded the predicted voltage-to-gap ratio due to the presence of a fast moving ionization wavefront [156]. Shortly thereafter, work was completed measuring the electric field of a diffuse nanosecond pulse discharge sustained in atmospheric pressure air for different applied voltages [169]. For all cases with a discharge present, the authors observed a significant overshoot of the Laplacian field by over an order of magnitude with a precipitous drop as the ionization wavefront passed the measurement location. Similar work, shown in figure 13, was then completed where the electric field was measured in fast ionization wave discharge at pressures ranging from 20–100 mbar (15–75 Torr) and the ionization wavespeed and amplitude was measured as a function of pressure [18]. Interestingly enough, the researchers observed during the calibration method that the measured signal intensity did not vary as a function of pressure as was expected. The researchers concluded that much of the generated signal was not generated in the gas, but rather in the walls of the discharge tube itself. This presents a new and exciting opportunity where one may now be able to access electric field measurements regardless of the process gas density or other experiment specific factors.

One final advancement in the E-FISH method has been the application of cylindrical focusing for 1D electric field imaging. This was first done by Goldberg *et al* [159] where a femtosecond laser was used to measure the electric field of an

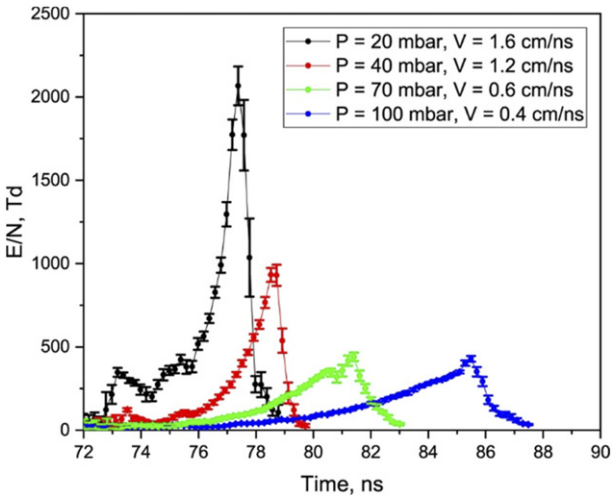


**Figure 13.** E-FISH measurements with the signal generated in the glass wall of the discharge tube as a function of pressure in fast ionization wave geometry. The characteristic field enhancement of the ionization wavefront is observed with the sharp drop due to plasma self shielding within the highly ionized discharge. Reproduced from [18]. 

atmospheric pressure plasma jet using argon as the process gas and a pure $N_2$ co-flow to shield the discharge from oxygen. Unfortunately, due to the discharge movement around the output of the core flow ceramic tube, absolute field measurements were quite low as many laser shots missed the discharge itself. The method has since been used in a 1D configuration to measure plasma uniformity and surface ionization wave propagation along a liquid surface by orienting the laser sheet parallel to the ground plane rather than perpendicular to it [160]. Finally, it has most recently been used in a similar, parallel to the ground plane, configuration to measure the onset of plasma thermal-chemical instabilities [170].

While the E-FISH method is clearly a powerful and widely applicable measurement technique, there are still several open questions which remain that must be considered in order to accurately interpret results. Primarily, recent work by Chng *et al* indicates that the spatial resolution is not accurately characterized by the Rayleigh range as originally suggested, but is instead significantly longer due to the higher intensities of focusing Gaussian beams [161]. Thus, for the most accurate calibration, the extent of the electric field with a plasma present must match the extent of the field during the calibration phase of an experiment. In practice, this is rarely precisely met although it can be close depending upon the discharge studied. Furthermore, recent work has been done independently comparing modeling results with E-FISH measurements, largely shown to be in good agreement despite possible variations between the extent of the calibration and measurement fields [171]. Additional follow on work by Chng *et al* [172] has simulated an E-FISH response and compared it to 'truth' data predicted by a 2D axisymmetric fluid simulation. In this work, the authors discovered that the overall shape of the field is relatively well captured by E-FISH and further outline a procedure which one may use to characterize the accuracy of E-FISH measurements.

An additional concern is the influence of charged and reactive species upon the calibration results. Reading carefully over E-FISH work, one notices the great lengths that researchers must go through in order to ensure that their calibration setup is as close as possible both with and without a plasma present. However, one can never precisely match the two as charged and reactive species can have an outsized influence on the net hyperpolarizability. One primary example of this could be product species generated during combustion, where the initial neutral population can be entirely replaced with varying species such as polar molecules like $H_2O$ or species with a larger hyperpolarizability than the calibration gasses such as $CO_2$. As of this writing, there has not yet been a comprehensive study into how such product species influence the E-FISH results. At present, most researchers typically use as all-encompassing a calibration method as possible and conclude that the calibration neutrals are still the dominant species.

Finally, determining when the pump laser pulse arrives with respect to the onset of breakdown is often a complicated process. All cables and measurement devices have inherent response times and delays which can influence the timing measured on the digital oscilloscope. In practice, the simplest method for determining the inherent time delays is using the rising edge of a sub-breakdown nanosecond HV pulse allowing for a calibrated $\Delta t$ measurement across all data taken with the same cables. Understanding the instant in time when breakdown occurs is additionally a difficult process often with a timing jitter on the same order as the measurement resolution. For this reason, most researchers are careful to indicate that their measurements are with respect to HV initiation rather than the precise moment when breakdown occurs. Alternatively, one can attempt to measure the time delay of every laser shot and average the results into time bins in a post-processing routine.

## 4. Closing remarks and outlook

Although the electric field strength is a basic plasma parameter there exists no universal method for its determination in transient plasmas. In air and helium or hydrogen containing discharges OES based methods has demonstrated its ability to determine electric field strength with high spatial and temporal resolution. This resolution is mainly limited by the imaging and/or time resolution of the detection system. However, ICCD and streak cameras as well as time-correlated single photon counting or fast PMTs offer sufficient time resolution. OES based methods are non-intrusive and relatively simple to apply. Its limitation is that there can be no information obtained when there is no emission. Another drawback is, that all these methods are based on distinct excitation schemes, which need a theoretical support. Although most studies are devoted to air or helium/hydrogen plasmas there is no general limitation since collision radiative schemes can be developed for any kind of system as long as two different radiative states with different energy threshold are directly excited in the discharge.

Laser based methods enable the electric field strength determination without emission from plasma and thus, also give information about the field configuration prior or after the discharge event. While LIF-DIP and E-CARS are limited to certain gases or gas mixtures, the E-FISH method became a powerful and widely applicable measurement technique within the last decade. It represents arguably the current state of the art for laser based transient electric field measurements. It is a relatively simple diagnostic which works in any gaseous species as well as with many commonly available laser systems. The time response of the method is determined entirely by the pump laser pulse duration. Pico- and even femtosecond resolution is achievable. From this viewpoint, E-FISH may become the standard for electric field strength measurements in the coming years. Therefore, several open questions like the spatial resolution and accuracy, calibration accuracy, the influence of local plasma chemistry and the temporal correlation between field development and the discharge event must be addressed. In this context, the other techniques described in this review could be used for an independent validation as well as in situation where laser radiation cannot be applied without disturbing the plasma.

Determining the electric field in transient plasmas remains a challenging and exciting field of plasma research.

## Acknowledgments

This work performed under the auspices of the U.S. Department of Energy by Lawrence Livermore National Laboratory under Contract DE-AC52-07NA27344 with document release number LLNL-JRNL-828828. BMG acknowledges the support of Dr Chamoire for numerous enlightening and fruitful discussions over the years. TH acknowledges the support of Czech Science Foundation Project GAČR No. 21-16391S and Project LM2018097 funded by the Ministry of Education, Youth and Sports of the Czech Republic. TH also acknowledges fruitful discussions with Milan Šimek, Detlef Loffhagen, Petr Bílek and Zdeněk Bonaventura. RB acknowledges support of German Science Foundation (DFG, 'Fundamentals of Complex Plasmas' and German Academic Exchange Service (DAAD, Grant 57218879) as well as Kirill V Kozlov, Hans-Erich Wagner, Detlef Loffhagen as well as Milorad Kuraica and his team and Belgrade University for cooperation and support.

## Data availability statement

No new data were created or analysed in this study.

## ORCID iDs

Benjamin M Goldberg https://orcid.org/0000-0002-1595-0450
Tomáš Hoder https://orcid.org/0000-0001-5346-6275
Ronny Brandenburg https://orcid.org/0000-0003-3153-8439

## References


[1] Adamovich I *et al* 2017 *J. Phys. D: Appl. Phys.* **50** 323001
[2] Weltmann K D *et al* 2019 *Plasma Processes Polym.* **16** 1800118
[3] Huxley L G H, Crompton R W and Elford M T 1966 *Phys. Bull.* **17** 251
[4] Huiskamp T, Beckers F J C M, van Heesch E J M and Pemen A J M 2016 *IEEE Sens. J.* **16** 3792–801
[5] Takashima K, Adamovich I V, Xiong Z, Kushner M J, Starikovskaia S, Czarnetzki U and Luggenhölscher D 2011 *Phys. Plasmas* **18** 083505
[6] Anikin N B, Starikovskaia S M and Starikovskii A Y 2002 *J. Phys. D: Appl. Phys.* **35** 2785–94
[7] Kawasaki T, Terashima T, Suzuki S and Takada T 1994 *J. Appl. Phys.* **76** 3724–9
[8] Zhu Y, Takada T and Tu D 1995 *J. Phys. D: Appl. Phys.* **28** 1468–77
[9] Li M, Li C, Zhan H, Xu J and Wang X 2008 *Appl. Phys. Lett.* **92** 031503
[10] Stollenwerk L, Laven J G and Purwins H-G 2007 *Phys. Rev. Lett.* **98** 255001
[11] Bogaczyk M, Wild R, Stollenwerk L and Wagner H-E 2012 *J. Phys. D: Appl. Phys.* **45** 465202
[12] Stollenwerk L 2009 *New J. Phys.* **11** 103034
[13] Bruggeman P and Leys C 2009 *J. Phys. D: Appl. Phys.* **42** 053001
[14] Tschiersch R, Nemschokmichal S, Bogaczyk M and Meichsner J 2017 *J. Phys. D: Appl. Phys.* **50** 105207
[15] Slikboer E, Garcia-Caurel E, Guaitella O and Sobota A 2017 *Plasma Sources Sci. Technol.* **26** 035002
[16] Slikboer E, Acharya K, Sobota A, Garcia-Caurel E and Guaitella O 2020 *Sci. Rep.* **10** 2712
[17] Robert E, Darny T, Dozias S, Iseni S and Pouvesle J M 2015 *Phys. Plasmas* **22** 122007
[18] Chng T L, Orel I S, Starikovskaia S M and Adamovich I V 2019 *Plasma Sources Sci. Technol.* **28** 045004
[19] Anikin N B, Pancheshnyi S V, Starikovskaia S M and Starikovskii A Y 1998 *J. Phys. D: Appl. Phys.* **31** 826–33
[20] Hoder T, Loffhagen D, Voráč J, Becker M M and Brandenburg R 2016 *Plasma Sources Sci. Technol.* **25** 025017
[21] Stephens J, Fierro A, Trienekens D, Dickens J and Neuber A 2014 *Plasma Sources Sci. Technol.* **24** 015013
[22] Winkler R, Loffhagen D and Sigeneger F 2002 *Appl. Surf. Sci.* **192** 50–71
[23] Makabe T and Petrovic Z L 2006 *Plasma Electronics: Applications in Microelectronic Device Fabrication* (Boca Raton, FL: CRC Press)
[24] Iza F, Kim G J, Lee S M, Lee J K, Walsh J L, Zhang Y T and Kong M G 2008 *Plasma Processes Polym.* **5** 322–44
[25] Tarasenko V F, Baksht E K, Beloplotov D V, Burachenko A G, Sorokin D A and Lomaev M I 2018 *J. Phys. D: Appl. Phys.* **51** 424001
[26] Chanrion O, Bonaventura Z, Çinar D, Bourdon A and Neubert T 2014 *Environ. Res. Lett.* **9** 055003
[27] Bruggeman P J, Iza F and Brandenburg R 2017 *Plasma Sources Sci. Technol.* **26** 123002
[28] Navrátil Z, Morávek T, Ráheľ J, Čech J, Lalinský O and Trunec D 2017 *Plasma Sources Sci. Technol.* **26** 055025
[29] Zhu X-M and Pu Y-K 2010 *J. Phys. D: Appl. Phys.* **43** 403001
[30] Obrusník A, Bílek P, Hoder T, Šimek M and Bonaventura Z 2018 *Plasma Sources Sci. Technol.* **27** 085013
[31] Bílek P, Obrusník A, Hoder T, Šimek M and Bonaventura Z 2018 *Plasma Sources Sci. Technol.* **27** 085012
[32] Dujko S, White R D and Petrović Z L 2008 *J. Phys. D: Appl. Phys.* **41** 245205
[33] Hoder T, Černák M, Paillol J, Loffhagen D and Brandenburg R 2012 *Phys. Rev.* E **86** 055401
[34] Braun D, Gibalov V and Pietsch G 1992 *Plasma Sources Sci. Technol.* **1** 166–74
[35] Kogelschatz U, Eliasson B and Egli W 1997 *J. Physique* **07** C4–66
[36] Kozlov K V, Wagner H-E, Brandenburg R and Michel P 2001 *J. Phys. D: Appl. Phys.* **34** 3164–76
[37] Jahanbakhsh S, Hoder T and Brandenburg R 2019 *J. Appl. Phys.* **126** 193305
[38] Kuo C-L *et al* 2005 *Geophys. Res. Lett.* **32** L19103
[39] Gharib M, Mendoza S, Rosenfeld M, Beizai M and Alves Pereira F J 2017 *Proc. Natl Acad. Sci. USA* **114** 12657–62
[40] Malagón-Romero A, Pérez-Invernón F J, Luque A and Gordillo-Vázquez F J 2019 *J. Geophys. Res.: Atmos.* **124** 12356–70
[41] Gallimberti I, Hepworth J K and Klewe R C 1974 *J. Phys. D: Appl. Phys.* **7** 880–98
[42] Creijghton Y .L .M 1994 Pulsed positive corona discharges: fundamental study and application to flue gas treatment *PhD Thesis* Eindhoven University of Technology
[43] Pancheshnyi S V, Starikovskaia S M and Starikovskii A Y 1999 *J. Phys. D: Appl. Phys.* **32** 2219–27
[44] Kozlov K V, Shepeliuk O and Samoilovich V 1995 Spatio-temporal evolution of the dielectric barrier discharge channels in air at atmospheric pressure *Proc.11th Int. Conf. Gas Discharges and their Applications* (Tokyo, Japan) vol 2 pp 142–5
[45] Matveev A A and Silakov V P 1998 Method of calculation of specific radiant emitting of the bands of 1- and 2+ systems of nitrogen in the non-equilibrium nitrogen–oxygen plasma *Physics and Technology of Electric Power Transmission* (Moscow: MPEI) pp 201–18
[46] Djakov A F, Bobrov Y K, Bobrova L N and Yourguelenas Y V 1998 Streamer discharge plasma parameters determination in air on a base of a measurement of radiation of the molecular bands of nitrogen *Physics and Technology of Electric Power Transmission* (Moscow: MPEI) pp 219–33
[47] Bonaventura Z, Bourdon A, Celestin S and Pasko V P 2011 *Plasma Sources Sci. Technol.* **20** 035012
[48] Celestin S and Pasko V P 2010 *Geophys. Res. Lett.* **37** L07804
[49] Naidis G V 2009 *Phys. Rev.* E **79** 057401
[50] Hoder T, Bonaventura Z, Bourdon A and Šimek M 2015 *J. Appl. Phys.* **117** 073302
[51] Stepanyan S A, Soloviev V R and Starikovskaia S M 2014 *J. Phys. D: Appl. Phys.* **47** 485201
[52] Dilecce G, Ambrico P F and De Benedictis S 2010 *J. Phys. D: Appl. Phys.* **43** 195201
[53] Hoder T, Šimek M, Bonaventura Z, Prukner V and Gordillo-Vázquez F J 2016 *Plasma Sources Sci. Technol.* **25** 045021
[54] Paris P, Aints M, Valk F, Plank T, Haljaste A, Kozlov K V and Wagner H-E 2005 *J. Phys. D: Appl. Phys.* **38** 3894–9
[55] Pancheshnyi S 2006 *J. Phys. D: Appl. Phys.* **39** 1708–10
[56] Paris P, Aints M, Valk F, Plank T, Haljaste A, Kozlov K V and Wagner H-E 2006 *J. Phys. D: Appl. Phys.* **39** 2636–9
[57] Dilecce G 2014 *Plasma Sources Sci. Technol.* **23** 015011
[58] Valk F, Aints M, Paris P, Plank T, Maksimov J and Tamm A 2010 *J. Phys. D: Appl. Phys.* **43** 385202
[59] Bílek P, Šimek M and Bonaventura Z 2019 *Plasma Sources Sci. Technol.* **28** 115011
[60] Hoder T, Synek P, Chorvát D, Ráhel' J, Brandenburg R and Černák M 2017 *Plasma Phys. Control. Fusion* **59** 074001
[61] Jánský J, Bessiéres D, Brandenburg R, Paillol J and Hoder T 2021 *Plasma Sources Sci. Technol.* **30** 105008
[62] Brisset A, Gazeli K, Magne L, Pasquiers S, Jeanney P, Marode E and Tardiveau P 2019 *Plasma Sources Sci. Technol.* **28** 055016

[63] Jõgi I, Levoll E, Paris P and Aints M 2016 Comparison of experimental and theoretical spectra of non-self-sustained discharge in nitrogen and air in wide range of field strength and pressure *Proc. 15th High Pressure Low Temperature Plasma Chemistry Symp.* (Brno, Czech Republic)

[64] Šimek M 2014 *J. Phys. D: Appl. Phys.* **47** 463001

[65] Shcherbakov Y V and Nekhamkin L I 2007 Computation and verification of the rate coefficients for spectral diagnostics of streamer discharges *2007 Annual Report—Conf. Electrical Insulation and Dielectric Phenomena* pp 751–4

[66] Kozlov K V and Wagner H-E 2007 *Contrib. Plasma Phys.* **47** 26–33

[67] Shcherbakov Y V and Sigmond R S 2007 *J. Phys. D: Appl. Phys.* **40** 460–73

[68] Shcherbakov Y V and Sigmond R S 2007 *J. Phys. D: Appl. Phys.* **40** 474–87

[69] Liu C, Fridman A and Dobrynin D 2019 *J. Phys. D: Appl. Phys.* **52** 105205

[70] Starikovskaia S M, Anikin N B, Pancheshnyi S V and Starikovskii A Y 2002 Time-resolved emission spectroscopy and its applications to the study of pulsed nanosecond high-voltage discharges *SPIE Proc. Selected Research Papers on Spectroscopy of Nonequilibrium Plasma at Elevated Pressures* vol 4460 pp 63–73

[71] Hoder T, Bonaventura Z, Prukner V, Gordillo-Vázquez F J and Šimek M 2020 *Plasma Sources Sci. Technol.* **29** 03LT01

[72] Pérez-Invernón F J, Luque A, Gordillo Vázquez F J, Sato M, Ushio T, Adachi T and Chen A B 2018 *J. Geophys. Res.: Atmos.* **123** 12917–41

[73] Nayak G, Du Y, Brandenburg R and Bruggeman P J 2017 *Plasma Sources Sci. Technol.* **26** 035001

[74] Starikovskaia S M, Allegraud K, Guaitella O and Rousseau A 2010 *J. Phys. D: Appl. Phys.* **43** 124007

[75] Starikovskii A Y, Nikipelov A A, Nudnova M M and Roupassov D V 2009 *Plasma Sources Sci. Technol.* **18** 034015

[76] Kosarev I N, Khorunzhenko V I, Mintoussov E I, Sagulenko P N, Popov N A and Starikovskaia S M 2012 *Plasma Sources Sci. Technol.* **21** 045012

[77] Dyatko N A, Ionikh Y Z and Meshchanov A V 2021 *Plasma Sources Sci. Technol.* **30** 055015

[78] Hoder T, Becker M and Loffhagen D 2019 Method for spectroscopic determination of sub-nanosecond electric field development in argon plasmas using a time-dependent line-ratio approach *APS Gaseous Electronics Conf.* p FT1.030

[79] Siepa S, Danko S, Tsankov T V, Mussenbrock T and Czarnetzki U 2014 *J. Phys. D: Appl. Phys.* **47** 445201

[80] Dyatko N A, Ionikh Y Z, Kalinin S A and Mityureva A A 2020 *Plasma Phys. Rep.* **46** 200–16

[81] Liu C Y, Cohen M B and Walker M L R 2020 *IEEE Trans. Plasma Sci.* **48** 1060–75

[82] Engeln R, Klarenaar B and Guaitella O 2020 *Plasma Sources Sci. Technol.* **29** 063001

[83] Brose E 1919 *Ann. Phys., Lpz.* **363** 731–52

[84] Takiyama K, Usui T, Kamiura Y, Fujita T, Oda T and Kawasaki K 1986 *Japan. J. Appl. Phys.* **25** L455

[85] Kuraica M M and Konjević N 1997 *Appl. Phys. Lett.* **70** 1521–3

[86] Mirzaee M, Simeni Simeni M and Bruggeman P J 2020 *Phys. Plasmas* **27** 123505

[87] Cvetanović N, Martinović M M, Obradović B M and Kuraica M M 2015 *J. Phys. D: Appl. Phys.* **48** 205201

[88] Sretenović G B, Krstić I B, Kovačević V V, Obradović B M and Kuraica M M 2011 Spectroscopic measurement of electric field in atmospheric-pressure plasma jet operating in bullet mode *Appl. Phys. Lett.* **99** 161502

[89] Booth J P, Derouard J, Fadlallah M and Sadeghi N 1993 *J. Appl. Phys.* **74** 862–7

[90] Ivković S S, Obradović B M, Cvetanović N, Kuraica M M and Purić J 2009 *J. Phys. D: Appl. Phys.* **42** 225206

[91] Obradović B M, Ivković S S and Kuraica M M 2008 *Appl. Phys. Lett.* **92** 191501

[92] Ivković S S, Obradović B M and Kuraica M M 2012 *J. Phys. D: Appl. Phys.* **45** 275204

[93] Sobota A *et al* 2016 *Plasma Sources Sci. Technol.* **25** 065026

[94] Wang Q, Koleva I, Donnelly V M and Economou D J 2005 *J. Phys. D: Appl. Phys.* **38** 1690–7

[95] Sismanoglu B N, Grigorov K G, Santos R A, Caetano R, Rezende M V O, Hoyer Y D and Ribas V W 2010 *Eur. Phys. J.* D **60** 479–87

[96] Čech J, Navrátil Z, Štipl M, Morávek T and Ráheľ J 2018 *Plasma Sources Sci. Technol.* **27** 105002

[97] Ivković S S, Sretenović G B, Obradović B M, Cvetanović N and Kuraica M M 2014 *J. Phys. D: Appl. Phys.* **47** 055204

[98] Navrátil Z, Josepson R, Cvetanović N, Obradović B and Dvořák P 2016 *Plasma Sources Sci. Technol.* **25** 03LT01

[99] Schultz A, Cruse H W and Zare R N 1972 *J. Chem. Phys.* **57** 1354–5

[100] Sinha M P, Schultz A and Zare R N 1973 *J. Chem. Phys.* **58** 549–56

[101] Gavrilenko V P 2006 *Instrum. Exp. Tech.* **49** 149–56

[102] Czarnetzki U, Luggenhölscher D and Döbele H F 1998 *Phys. Rev. Lett.* **81** 4592–5

[103] Czarnetzki U, Luggenhölscher D and Döbele H F 1999 *Plasma Sources Sci. Technol.* **8** 230–48

[104] Eckbreth A C 1996 *Laser Diagnostics for Combustion Temperature and Species* (Boca Raton, FL: CRC Press)

[105] Kinsey J L 1977 *Annu. Rev. Phys. Chem.* **28** 349–72

[106] Gavrilenko V P, Kim H J, Ikutake T, Kim J B, Choi Y W, Bowden M D and Muraoka K 2000 *Phys. Rev.* E **62** 7201–8

[107] Barnat E V and Hebner G A 2007 *J. Appl. Phys.* **101** 013306

[108] Czarnetzki U, Hebner G A, Luggenholscher D, Dobele H F and Riley M E 1999 *IEEE Trans. Plasma Sci.* **27** 70–1

[109] Wagenaars E, Bowden M D and Kroesen G M W 2007 *Phys. Rev. Lett.* **98** 075002

[110] Wagenaars E, Kroesen G M W and Bowden M D 2006 *Phys. Rev.* A **74** 033409

[111] Barnat E V and Hebner G A 2004 *Appl. Phys. Lett.* **85** 3393–5

[112] Ganguly B N and Garscadden A 1985 *Phys. Rev.* A **32** 2544–5

[113] Barnat E V and Hebner G A 2005 *J. Appl. Phys.* **98** 013305

[114] Choi Y W, Bowden M D and Muraoka K 1996 *Appl. Phys. Lett.* **69** 1361–3

[115] Booth J P, Fadlallah M, Derouard J and Sadeghi N 1994 *Appl. Phys. Lett.* **65** 819–21

[116] Greenberg K E and Hebner G A 1993 *Appl. Phys. Lett.* **63** 3282–4

[117] Barnat E V and Hebner G A 2004 *J. Appl. Phys.* **96** 4762–70

[118] Takizawa K, Sasaki K and Kono A 2004 *Appl. Phys. Lett.* **84** 185–7

[119] Schulze J, Heil B G, Luggenhölscher D, Brinkmann R P and Czarnetzki U 2008 *J. Phys. D: Appl. Phys.* **41** 195212

[120] Kampschulte T, Schulze J, Luggenhölscher D, Bowden M D and Czarnetzki U 2007 *New J. Phys.* **9** 18

[121] Chen T Y, Goldberg B M, Patterson B D, Kolemen E, Ju Y and Kliewer C J 2020 *Opt. Lett.* **45** 4252–5

[122] Kearney S P 2015 *Combust. Flame* **162** 1748–58

[123] Lempert W R and Adamovich I V 2014 *J. Phys. D: Appl. Phys.* **47** 433001

[124] Bohlin A and Kliewer C J 2013 *J. Chem. Phys.* **138** 221101

[125] Bohlin A and Kliewer C J 2014 *Appl. Phys. Lett.* **104** 031107

[126] Kearney S P, Scoglietti D J and Kliewer C J 2013 *Opt. Express* **21** 12327–39

[127] Ochkin V N and Tskhai S N 2003 *Phys.-Usp.* **46** 1214

[128] Lempert W R, Kearney S P and Barnat E V 2011 *Appl. Opt.* **50** 5688–94
[129] Kulatilaka W D, Hsu P S, Stauffer H U, Gord J R and Roy S 2010 *Appl. Phys. Lett.* **97** 081112
[130] Tskhai S N, Akimov D A, Mitko S V, Ochkin V N, Serdyuchenko A Y, Sidorov-Biryukov D A, Sinyaev D V and Zheltikov A M 2001 *J. Raman Spectrosc.* **32** 177–81
[131] Ito T, Kobayashi K, Czarnetzki U and Hamaguchi S 2010 *J. Phys. D: Appl. Phys.* **43** 062001
[132] van der Schans M, Böhm P, Teunissen J, Nijdam S, IJzerman W and Czarnetzki U 2017 *Plasma Sources Sci. Technol.* **26** 115006
[133] Simeni Simeni M, Goldberg B M, Zhang C, Frederickson K, Lempert W R and Adamovich I V 2017 *J. Phys. D: Appl. Phys.* **50** 184002
[134] Böhm P, Kettlitz M, Brandenburg R, Höft H and Czarnetzki U 2016 *Plasma Sources Sci. Technol.* **25** 054002
[135] Goldberg B M, Shkurenkov I, O'Byrne S, Adamovich I V and Lempert W R 2015 *Plasma Sources Sci. Technol.* **24** 035010
[136] Goldberg B M, Böhm P S, Czarnetzki U, Adamovich I V and Lempert W R 2015 *Plasma Sources Sci. Technol.* **24** 055017
[137] Simeni Simeni M, Baratte E, Hung Y-C, Frederickson K and Adamovich I V 2019 *Proc. Combust. Inst.* **37** 1497–504
[138] Simeni M S, Baratte E, Zhang C, Frederickson K and Adamovich I V 2018 *Plasma Sources Sci. Technol.* **27** 015011
[139] Gavrilenko V P *et al* 1992 *Sov. J. Exp. Theor. Phys. Lett.* **56** 1
[140] Evsin O A, Kupryanova E B, Ochkin V N, Savinov S Y and Tskhai S N 1995 *Quantum Electron.* **25** 278
[141] Akimov D A, Zheltikov A M, Koroteev N I, Naumov A N, Serdyuchenko A Y, Sidorov-Biryukov D A, Fedotov A B, Ochkin V N and Tskhai S N 1999 *JETP Lett.* **70** 375–9
[142] Kochanov V P and Bogdanova Y V 2003 *J. Exp. Theor. Phys.* **96** 202–21
[143] Goldberg B M, Shkurenkov I, Adamovich I V and Lempert W R 2016 *Plasma Sources Sci. Technol.* **25** 045008
[144] Simeni Simeni M, Tang Y, Frederickson K and Adamovich I V 2018 *Plasma Sources Sci. Technol.* **27** 104001
[145] Marko K A and Rimai L 1979 *Opt. Lett.* **4** 211–3
[146] Klick D, Marko K A and Rimai L 1981 *Appl. Opt.* **20** 1178–81
[147] Sitz P and Yaris R 1968 *J. Chem. Phys.* **49** 3546–57
[148] Franken P A, Hill A E, Peters C W and Weinreich G 1961 *Phys. Rev. Lett.* **7** 118–9
[149] Finn R S and Ward J F 1971 *Phys. Rev. Lett.* **26** 285–9
[150] Singer K D and Garito A F 1981 *J. Chem. Phys.* **75** 3572–80
[151] Shelton D P and Buckingham A D 1982 *Phys. Rev.* A **26** 2787–98
[152] Kielich S 1968 *Chem. Phys. Lett.* **2** 569–72
[153] Ward J F and Bigio I J 1975 *Phys. Rev.* A **11** 60–6
[154] Feng T, Raabe N, Rustige P and Steinmeyer G 2018 *Appl. Phys. Lett.* **112** 241101
[155] Dogariu A, Goldberg B M, O'Byrne S and Miles R B 2017 *Phys. Rev. Appl.* **7** 024024
[156] Goldberg B M, Chng T L, Dogariu A and Miles R B 2018 *Appl. Phys. Lett.* **112** 064102
[157] Retter J E and Elliott G S 2019 *Appl. Opt.* **58** 2557–66
[158] Simeni Simeni M, Tang Y, Hung Y-C, Eckert Z, Frederickson K and Adamovich I V 2018 *Combust. Flame* **197** 254–64
[159] Goldberg B M, Reuter S, Dogariu A and Miles R B 2019 *Opt. Lett.* **44** 3853–6
[160] Orr K, Tang Y, Simeni Simeni M, van den Bekerom D and Adamovich I V 2020 *Plasma Sources Sci. Technol.* **29** 035019
[161] Chng T L, Starikovskaia S M and Schanne-Klein M-C 2020 *Plasma Sources Sci. Technol.* **29** 125002
[162] Cui Y, Zhuang C and Zeng R 2019 *Appl. Phys. Lett.* **115** 244101
[163] Chng T L, Ding C, Naphade M, Goldberg B M, Adamovich I V and Starikovskaia S M 2020 *J. Instrum.* **15** C03005
[164] Chng T L, Naphade M, Goldberg B M, Adamovich I V and Starikovskaia S M 2020 *Opt. Lett.* **45** 1942–5
[165] Adamovich I V, Butterworth T, Orriere T, Pai D Z, Lacoste D A and Cha M S 2020 *J. Phys. D: Appl. Phys.* **53** 145201
[166] Lepikhin N D, Luggenhölscher D and Czarnetzki U 2020 *J. Phys. D: Appl. Phys.* **54** 055201
[167] Huang B, Zhang C, Adamovich I, Akishev Y and Shao T 2020 *Plasma Sources Sci. Technol.* **29** 044001
[168] Orr K, Yang X, Gulko I and Adamovich I V 2020 *Plasma Sources Sci. Technol.* **29** 125022
[169] Chng T L, Brisset A, Jeanney P, Starikovskaia S M, Adamovich I V and Tardiveau P 2019 *Plasma Sources Sci. Technol.* **28** 09LT02
[170] Rousso A C, Goldberg B M, Chen T Y, Wu S, Dogariu A, Miles R B, Kolemen E and Ju Y 2020 *Plasma Sources Sci. Technol.* **29** 105012
[171] Zhu Y, Chen X, Wu Y, Hao J, Ma X, Lu P and Tardiveau P 2021 *Plasma Sources Sci. Technol.* **30** 075025
[172] Chng T L, Pai D Z, Guaitella O, Starikovskaia S M and Bourdon A 2022 *Plasma Sources Sci. Technol.* **31** 015010